Copernicus assisted environmental monitoring across the Black Sea Basin - PONTOS

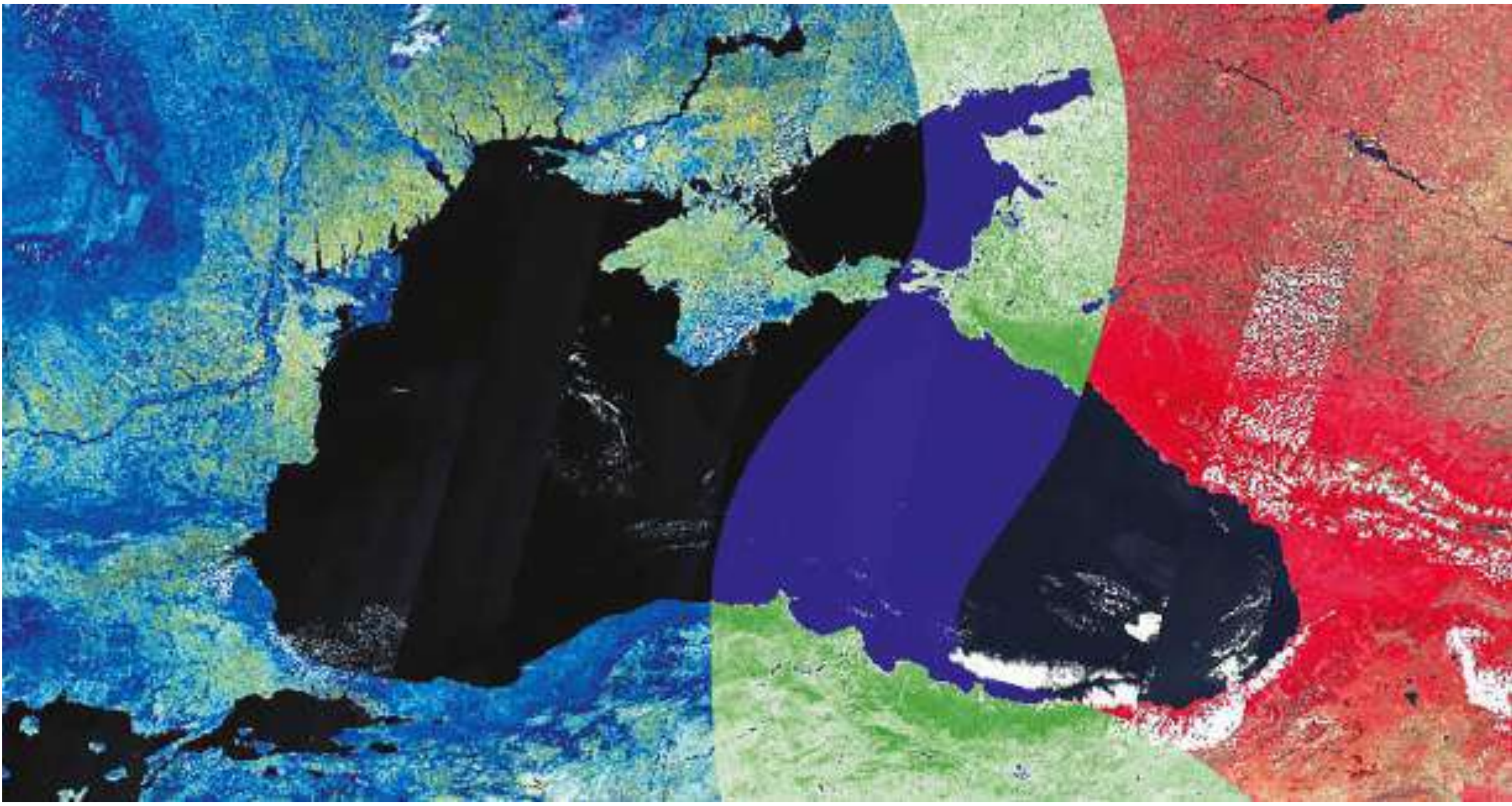

Agricultural water balance, water productivity, and water stress indices

Deliverable D.T1.2.6

PONTOS-GR (Greece)

Table of Contents

1 Introduction

It is well known that water scarcity stands as one of the most important limiting factors for the agricultural sector jeopardizing optimum production (Zamani et al., 2019; Linker et al., 2016). According to the latest reports, irrigation is accountable for the 51.4% and 59% of the total freshwater consumption in USA and EU, respectively (EEA, 2019; Maupin et al., 2014), whilst a further increase in irrigation water demands up to 30% is expected by 2030 (Beddington, 2009).

Moreover, the latest climate change IPCC scenarios have indicated that the Mediterranean Sea is one of the few regions globally in which climate change models project declines in precipitation depth, especially during the winter months, with an estimated potential reduction up to 40%. For this reason, the area is considered as a climate change “hot-spot” (Tuel and Eltahir, 2020). This shift in precipitation patterns is expected to affect mainly the winter rainfed crops (Abd-Elmabod et al., 2020). In parallel, an expected increase in the mean annual air temperature between 1-1.5 °C by 2040, in combination with prolonged heat-waves and consecutive drought periods are expected to substantially increase the irrigation water needs of spring-summer crops (Todaro et al., 2022). Recent studies conducted within Mediterranean borders, showed that the cumulative impacts of the above-mentioned effects may lead to a significant decrease in the available quantities of surface and groundwater resources (Rocha et al., 2020), posing a threat on food production security and the sustainability of the agricultural sector.

Coastal river deltas and their broader areas, usually serve as areas of intense agricultural exploitation, industry, and commerce (Loucks, 2019). Consequently, the pressure imposed to these complex and sensitive areas by the daily human socioeconomic activities results to their degradation by e.g., the overexploitation of groundwater resources leading to the salinization of coastal aquifers (Nguyen et al., 2019; Rahman et al. 2019), nutrients’ leaching (nitrogen, phosphorus) (Mai et al., 2010) and pesticides/herbicides substances from the agricultural land to the water resources (Papadopoulou-Mourkidou et al., 2003; Vryzas et al., 2009, 2011). Surface runoff and deep percolation (e.g., irrigation/rainfall water infiltration below plants’ rooting depth) are the main mechanisms of nutrient and pesticide leaching. Both mechanisms are the result of overirrigation or extreme rainfalls.

Recent studies have shown the potential of crop growth models to be used as irrigation scheduling tools, contributing to the rational use of the available water resources, securing the agricultural sector sustainability and increasing its resilience in the ongoing changes (Tsakmakis et al., 2017; Pereira et al., 2020). However, crop models have an innate level of uncertainty, due to the differences among crop cultivars and potential divergence in plants’ response to different soils and climate conditions. New generations of low-cost and reliable meteorological stations and soil moisture sensors, monitoring the climate conditions and soil moisture levels almost in real time, in combination with the advances in satellite remote sensing images, in terms of temporal and spatial resolution, promise to ameliorate the crop models uncertainty via an operational, in season correction and re-adjustment (Tsakmakis et al., 2021).

However, one of the main drawbacks of the crop models is that most of them perform point-based simulations (Tenreiro et al., 2020). This fact renders their value for region level estimations. To bridge this gap some researchers proposed and studied the coupling of crop models with hydrological models (e.g., Hydrus) (Siad et al., 2019). Nevertheless, hydrological models demand a significant number of inputs, whose determination requires field soil sampling and analysis, rendering their watershed level implementation unfeasible. On the other hand, the contemporary developments in remote sensing imagery, allowed the upscaling from single point modeling into regional scale calculations by exploiting the spatial distribution of vegetation indices (e.g., Normalized Difference Vegetation Index, NDVI) within a region (Bellón et al., 2017; Han et al., 2020). The acquired remote sensing images in combination with in-situ observations and advanced programming techniques (e.g., machine learning and deep learning) allow (a) the production of reliable regional crop maps (Frolking et al., 2002; Kussul et al., 2017; Wardlow and Egbert, 2008) or/and (b) the transformation of vegetation indices to plant development indices, such as the Leaf Area Index and the Green Canopy Cover (CC) (Ashapure et al., 2019; Prathumchai et al., 2018; Tsakmakis et al., 2021a; Veerakachen and Raksapatcharawong, 2020; Xu et al., 2019). The latter can be used as crop model validation parameters making possible their performance evaluation in watershed level.

Taking into consideration the inelastic and urgent needs to cope with the water scarcity and climate change challenges, EU new Common Agricultural Policy (CAP) 2023-2027 revised fundamentally the subsidies' philosophy, giving now a strong emphasis on results and performance (Heyl et al., 2021). In this context, the new CAP introduced the term "*conditionality*" meaning that a farmer must achieve certain predefined environmental performance targets (as defined within the submitted specific member states CAP strategic plans) if to get subsidies. Moreover, to encourage local initiatives and further reduce the agriculture sector environmental footprint, new CAP's "*eco-schemes*" allow, e.g., farmer partnerships, to set performance goals even beyond these defined by "*conditionality*" and claim extra subsidies by achieving them.

Thus, well-defined and scientifically sound indices are needed to assess the farmers' performance and judge if they achieve their targets (and receive subsidies) or not. In the case of irrigation water consumption, Water Footprint (WF) can be used as such an index. WF is defined as the water that is consumed during the production process of a good or the provision of a certain service, in the framework of our everyday socio-economic activities (Hoekstra, 2017; Hoekstra and Mekonnen, 2012). For the agricultural sector and specifically the soil cultivation for crop growing, WF is defined as the total amount of water that is evapotranspirated during a crop's growing season against the tradable weight of the crop's final product (Chukalla et al., 2015; Tsakmakis et al., 2018). Since 2015, WF has been used as an evaluation index in several studies to access the water use efficiency in river basin or watershed level (Cao et al., 2014; D'Ambrosio et al., 2020; Karandish et al., 2015; Zeng et al., 2012; Zhuo et al., 2016), as well as the means to assess the potential of the various irrigation system technologies, field management practices and irrigation strategies to reduce crop WF (Chukalla et al., 2015; Nouri et al., 2019; Tsakmakis et al., 2018).

Taking into consideration all the above, the coastal, deltaic part of Nestor River watershed in northern Greece was selected as the Greek study area to be analyzed in the framework of the Task "*Agricultural water balance, water productivity, and water stress indices*" of the PONTOS project funded by the Operational Program of the Black Sea Basin. For this purpose, three popular, water demanding arable crops that are cultivated within the study area, named maize, cotton and rice were selected among the various crops. This selection was based on the fact that crop models have been proved to be able to simulate with satisfactory accuracy the selected crops growing cycle and response to water stress conditions. Successively, data about the total cultivated area of each of the selected crops, as well as information about the weather conditions prevailing in the area (data from the Chrisoupolis Airport), and available soil data were collected from national repositories. Additionally, NDVI maps acquired from Copernicus Sentinel 2 mission, were used to estimate the plants' development curves, while interviews with farmers were conducted to gather practices about common field management and irrigation. The collected data were fed to a crop model named AquaCrop and the water footprint of the selected crops was estimated. The main objectives of the analysis were (a) to produce maps of vegetation indices, using satellite imagery data and evaluate the implemented irrigation schedules to derive the canopy cover (CC) time series; (b) use a crop model to estimate the actual WF of the most popular crops, using typical farmer empirical irrigation schedules; and (c) define the benchmark WF for the most popular crops implementing optimum irrigation schedules and compare them with the corresponding actual WF values.

2 Methodology

The high-level schema of the methodology architecture followed in this study is illustrated in Figure 1. In brief, soil, weather, satellite, crop and irrigation data were collected and fed to the AquaCrop crop model. The various sources that the data were collected from, as well as the required transformations which were performed to them, were described in detail in the following sub-sections.

Once all the data was collected and transformed to the proper format, they were fed to the AquaCrop crop model. The model simulated the crop's growing cycle, by solving the daily water balance of the plant-soil-atmosphere continuum, integrating the potential impacts of water stress conditions that the plants may experience during the various growing stages, interpreting them, e.g., as a reduction in biomass or/and final yield production.

Finally, the model results were used to assess the implemented irrigation schedule efficiency via the WF index. In this study, the green and blue components of WF were estimated, whilst the grey component was excluded, due to the lack of the required data to assess it. A set of benchmark WF values were derived for each crop, including aspects of the soil hydraulic characteristics.

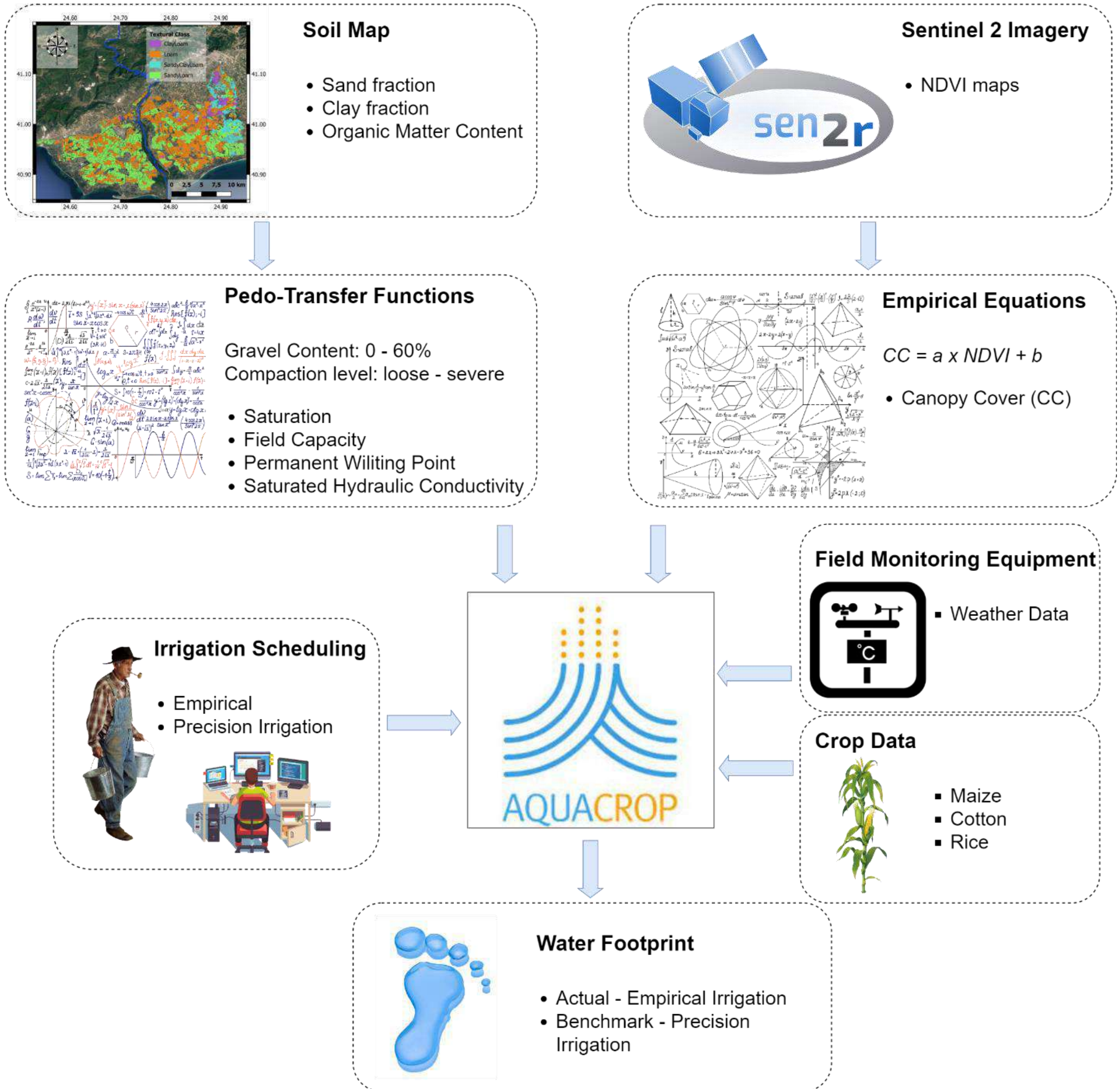

Figure 1. High-level schema of the implemented methodology.

2.1 Study Site Description

2.1.1 Soil Data

The Greek study site consisted of the coastal, plain part of the Nestos River watershed in northern Greece. It covers a total area of roughly 43,818 ha, spreading from 41.03°N to 40.85°N and 22.55°E to 24.85°E (Figure 2). From this area approximately 12,700 ha are cultivated, divided into 32,449 fields, with an average size of 0.9 ha.

The available regional soil map provided information about the sand and clay fractions, as well as the soil organic matter content of the study area fields. When the fields were classified based on USDA classification triangle, it was revealed that the eastern side of the Nestos River basin is dominated by loams and sandy loams (Figure 2). In the western side of the riverbank, loams and sandy loams are still present covering the largest portion of the land, but clay loams and sandy clay loams appear as well near the eastern border of the basin. Throughout the study area, sandy loams and loams cover an area of 11,555 ha and 13,020 ha, respectively, which correspond to roughly 41% and 57% of the total area (Table 1).

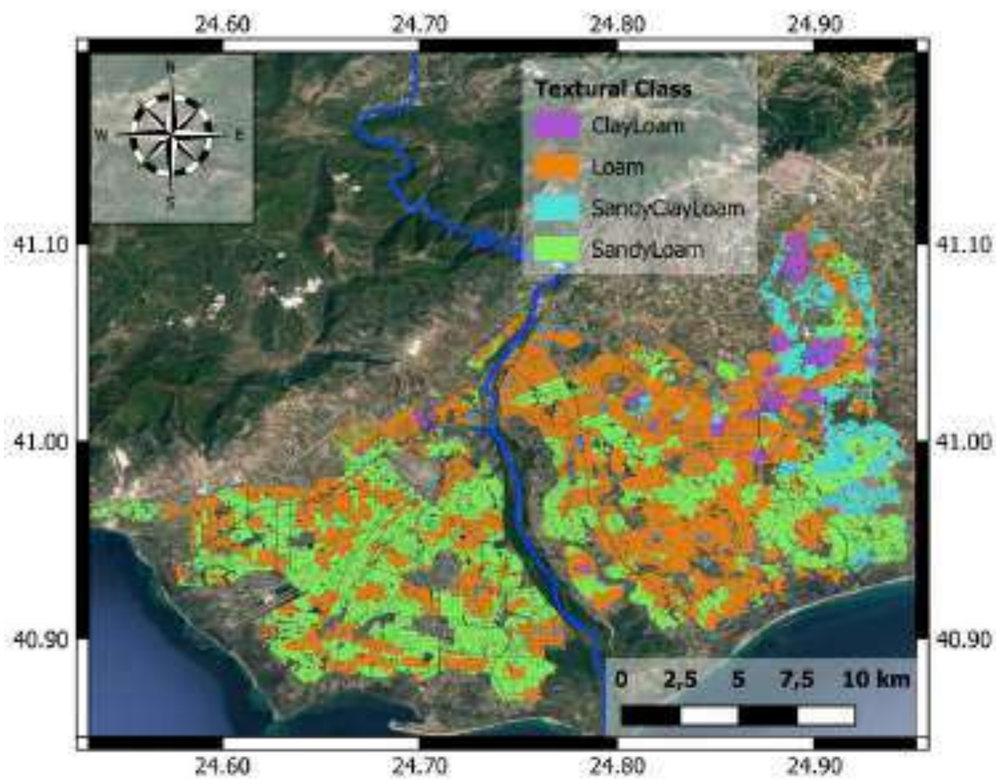

Figure 2. Soil textural class distribution within study area. Coordinates are in EPSG:4326 system.

Table 1. Main textural classes within the Greek study area.

Textural Class	Area (ha)	ATB (%)
Clay Loam	923.77	3.28
Loam	13,019.57	57.00
Sandy Clay Loam	2,329.12	8.27
Sandy Loam	11,555.42	41.02

ATB = textural class Area as percentage of the Total Basin cover

Despite the fact that many fields were classified within the same textural class, significant variations on the sand, clay and organic matter content were observed (Figure 2). In the case of sandy loam and loam textural classes, the mean value of the sand fraction was found to be roughly 59% ± 5.8 and 45% ± 6.11%, respectively (Table 2), with a substantial number of fields characterized as outliers, as they located outside the upper and lower whiskers of the box plots. Accordingly, the mean sand content for sandy clay loam and clayey loam classes were 55% ± 5.34 and 37% ± 6, respectively, but strikingly lower outliers were observed, located mainly outside the lower whisker bar.

The mean clay content for the sandy loam, loam, sandy clay loam and clayey loam classes was found to be 31% ± 2.62, 16% ± 3.82, 24% ± 3.37 and 32% ± 4.2, respectively (Table 2). Again, a considerable number of outliers was observed in the case of sandy loam and loam classes, while lower outliers were counted for sandy clay loam and clay loam classes, located outside the upper whisker bar this time (Figure 3).

The maximum and minimum values of the organic matter content were found to be very similar for all the textural classes (Table 1), ranging from roughly 0.2% to 3.9%. In general, the mean organic matter value showed an increase from the lighter to heavier soils (1.21% and 2.03% for sandy loam and clay loam, respectively).

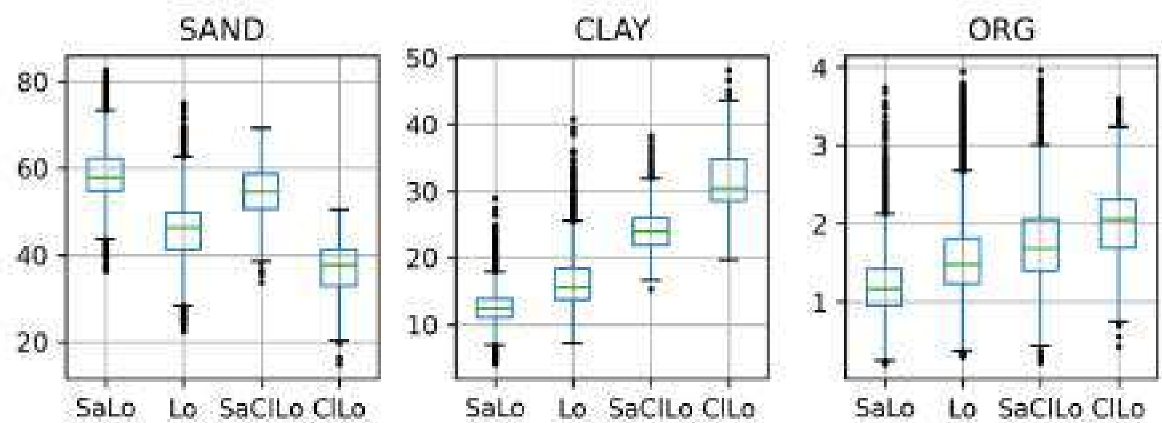

Figure 3. Variability of sand, clay, and organic matter content within the various textural classes. *SaLo = Sandy Loam; Lo = Loam; SaClLo = Sandy Clay Loam; ClLo= Clay Loam*

Table 2. Statistics of sand, clay and organic matter content within the various textural classes.

	SaLo	Lo	SaClLo	ClLo
		Sand (%)		
Mean	58.84	45.39	54.72	36.80
SD	5.84	6.11	5.34	6.03
Min	36.29	22.66	33.75	15.00
Q1 (25%)	54.78	41.29	50.66	32.87
Q3 (75%)	62.21	49.86	58.72	41.25
Max	82.51	74.88	69.26	50.53
		Clay (%)		
Mean	12.59	16.47	24.41	31.59
SD	2.62	3.82	3.37	4.20
Min	4.06	7.23	15.29	19.78
Q1 (25%)	11.03	13.74	21.93	28.58
Q3 (75%)	13.80	18.47	25.94	34.72
Max	28.98	40.88	38.40	48.15
		Organic Matter (%)		
Mean	1.21	1.56	1.72	2.03
SD	0.39	0.49	0.52	0.48
Min	0.20	0.30	0.22	0.43
Q1 (25%)	0.95	1.23	1.40	1.69
Q3 (75%)	1.42	1.81	2.05	2.311
Max	3.74	3.95	3.96	3.60

SaLo = Sandy Loam; Lo = Loam; SaClLo = Sandy Clay Loam; ClLo= Clay Loam

2.1.1.1 Soil hydraulic properties

Crop model simulations demand soil hydraulic properties. Thus, as long as the available data contain the sand-clay fractions and the organic matter content per field, pedo-transfer functions were implemented to obtain the required saturation point (SP), field capacity (FC), permanent wilting point (PWP) and saturated hydraulic conductivity (Ksat) (Saxton and Rawls, 2006). Except for the available sand-clay fractions and organic matter, the pedo-transfer functions demand as inputs the soil gravel content (GC) and the soil compaction level (SCL). As these data were not available, the following hypothetical scenarios were created and implemented to evaluate the impact of GC and SCL variations to the soil hydraulic parameters and thus the crop model output results.

Table 3. Hypothetical gravel content values and soil compaction level scenarios.

Gravel Content (%)	Soil Compaction Level
0	Normal
10	Normal
20	Normal
30	Normal
40	Normal

50	Normal
60	Normal
0	Loose
0	Dense
0	Hard
0	Severe

2.1.2 Crop Data

According to the national 2018, 2019 and 2020 crop maps, in the study area approximately 33,918 ha, 34,086 ha and 34,529 ha were cultivated, respectively. Irrigated maize was the most popular crop for all years, covering roughly 21-24% of the total cultivated land, 8,000 ha on average (Table 4). Cotton and rice covered a significantly lower portion of land, between 2% and 6%, occupying approximately an area of 660 to 2,289 ha.

Table 4. Popular arable water demanding crops cultivated within study area in 2018, 2019 and 2020.

Crop	2018		2019		2020	
	TCA (ha)	RA (%)	TCA (ha)	RA (%)	TCA (ha)	RA (%)
Maize	8,254	24.00	8,045	23.60	7,336	21.25
Cotton	1,567	4.62	2,289	6.72	1,994	5.77
Rice	924	2.72	664	1.95	715	2.07

TCA = Total Crop Area; RA = Relative Area as Total Crop Area/Total Area

The crop maps (Figures 4, 5 and 6) showed that the distribution pattern of the maize, cotton and rice fields was almost identical over the years. In general, maize was cultivated at both sides of the riverbank, preferably in sandy loam and loam soils. Almost all rice fields were located at the north-western plains of the study area, close to the coastline (Loam, Sandy Loam fields), probably due to the water supply canals network infrastructure that exists in this region allowing the easy flood of fields with water. On the other hand, cotton fields were observed mostly to the eastern side of the riverbank, being cultivated also on heavy soils e.g., clay loams and sandy clay loams.

2.1.2.1 Crop modeling parameters

In the case of maize crop, the crop file that was created and used as inputs to the AquaCrop model were based on experimental results conducted on the broader area of East Macedonia and Thrace (Tsakmakis et al., 2021). As local experimental data for the rice and cotton crop are not available, data from studies carried out in areas with similar weather conditions were exploited to create a rice crop file for the current work. Table 5 presents the values used for each key parameter.

Table 5. AquaCrop model calibrated values for the non-conservative and conservative parameters, as modified in the maize crop default file during the calibration process.

Parameter	Maize
Non-Conservative Parameters	
Initial Canopy cover, CCo (%)	0.44
Maximum canopy cover (%)	84.00
Maximum Rooting depth (m)	0.60
Minimum Effective Rotting Depth (m)	0.15
Canopy Growth Coefficient (%/day)	18.00
Canopy Decline Coefficient (%/GDD)	0.49
Base Temperature (°C)	10.00
Conservative Parameters	
Crop coefficient for transpiration (Kcb)	1.03
Reference Harvest Index (%)	63.00
Upper threshold below which leaf expansion is not optimal (p_{upper})	0.20
Lower threshold below which leaf expansion is halted (p_{lower})	0.74
Shape factor of water stress curve (f_{shape})	2.50

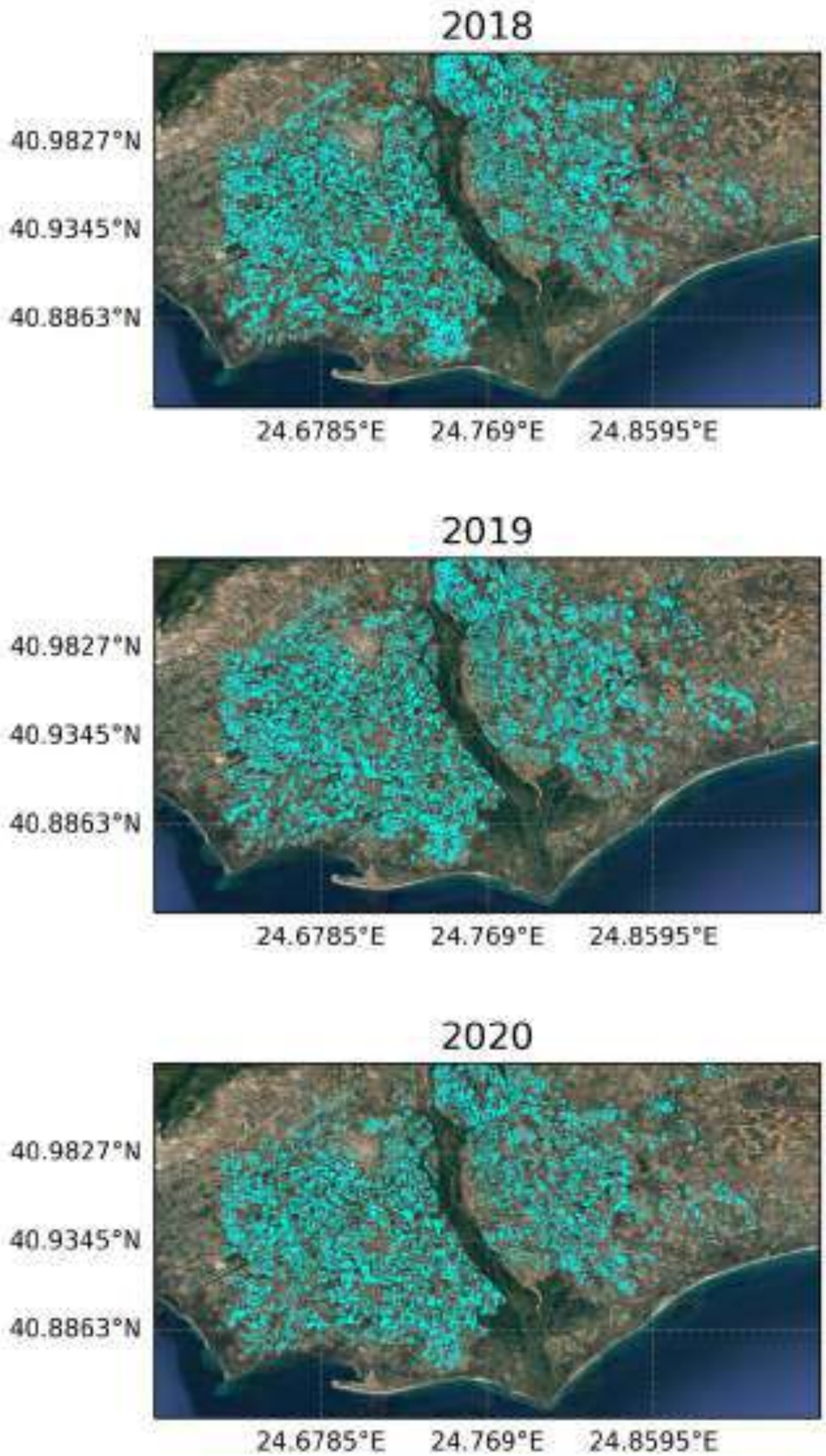

Figure 4. Fields cultivated with maize within the study area in 2018, 2019 and 2020.

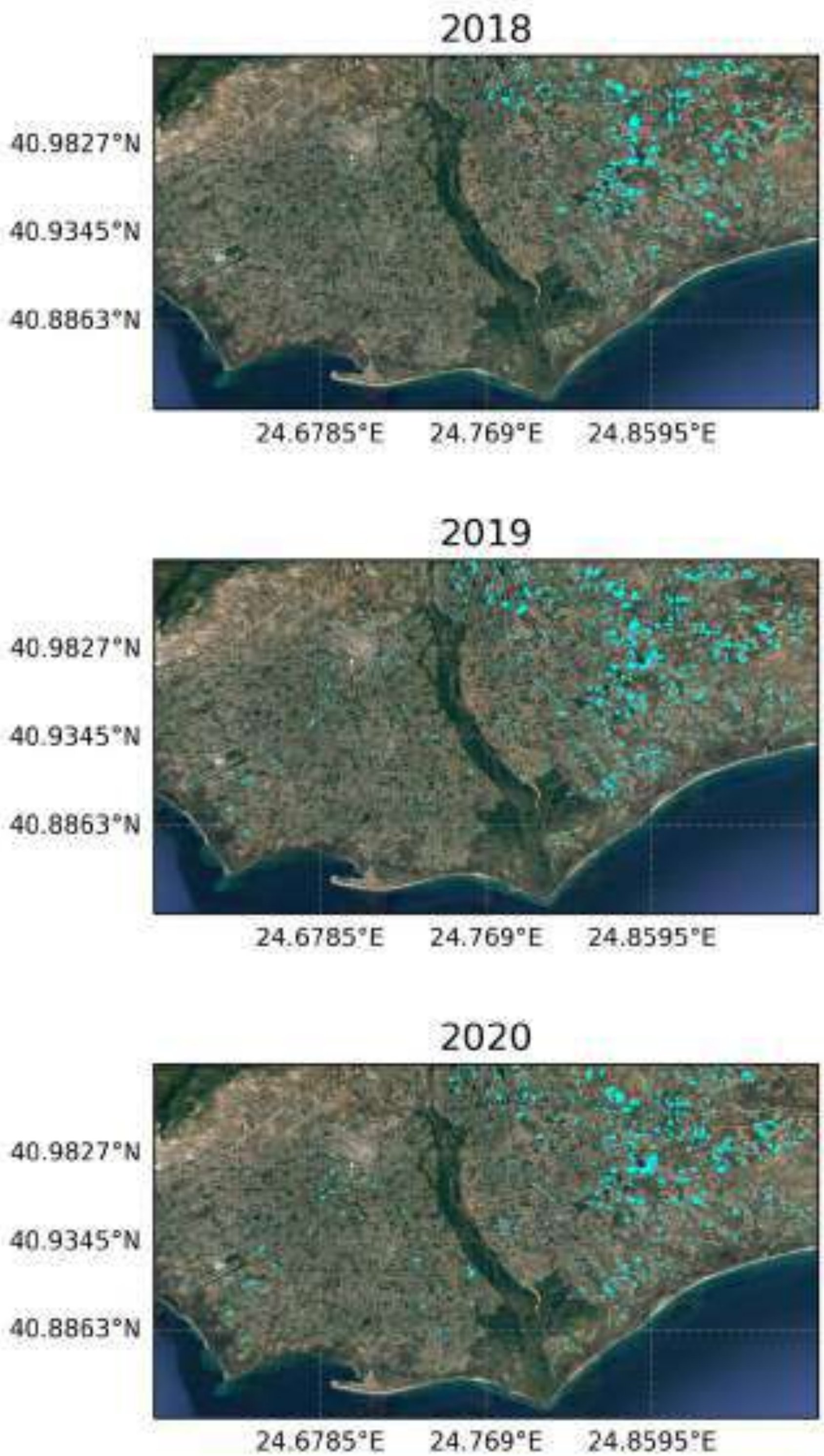

Figure 5. Fields cultivated with cotton within the study area in 2018, 2019 and 2020.

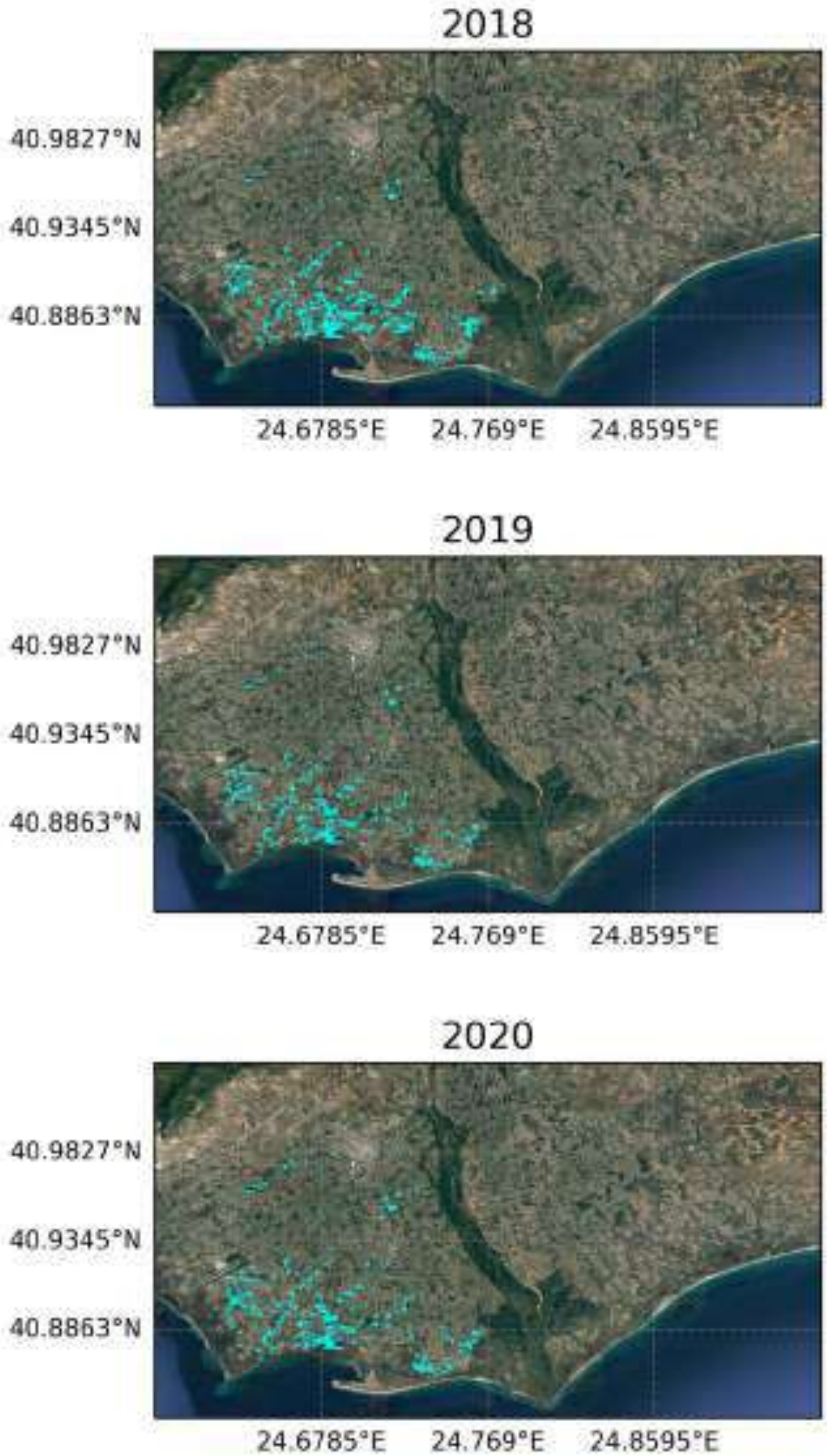

Figure 6. Fields cultivated with rice within the study area in 2018, 2019 and 2020.

2.1.3 Weather conditions

Between the years 2015-2020 the mean air temperature in the study area ranged from 15.2 to 16.2 °C, showing a slight upward trend (Table 6; Figure 7). During the early morning hours of January and February, the air temperature dropped below zero, with values up to -7.8 °C in 2016. On the other hand, the maximum air temperature values were observed in July and August, exceeding 35 °C in all years, with the absolute maximum of 37.8 °C, recorded in 2017.

Table 6. Minimum, mean and maximum air temperature records between 2015-2020 in the Greek study area.

Year	Air Temperature (C°)		
	Minimum	Mean	Maximum
2015	-6.4	15.5	35.4
2016	-7.8	15.8	36.6
2017	-6.0	15.2	37.8
2018	-5.0	16.1	35.8
2019	-6.2	16.2	36.4
2020	-4.6	16.0	35.6

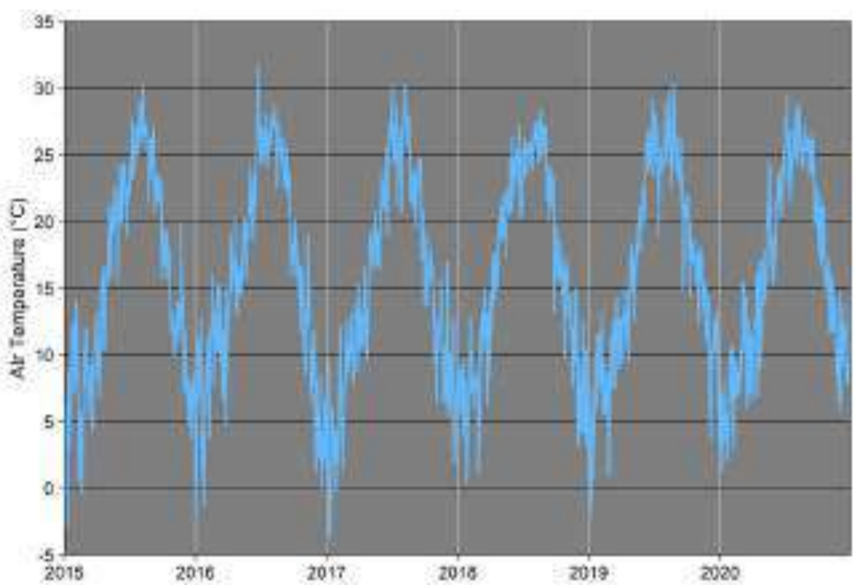

Figure 7. Air temperature annual fluctuations between years 2015-2020.

The annual cumulative rain depth showed a significant variation among years, from 322 mm in 2016 up to 766 mm in 2019 (Table 7; Figure 8). However, rainfall changes between the years were abrupt and do not reveal any obvious upward or downward trend. It is worth mentioning that from 2018 to 2020 at least two extreme events were recorded, exceeding 90 mm of rain water within a day (Table 5).

Table 7. Annual cumulative and daily maximum rain records between 2015-2020 in the Greek study area.

Year	Rain (mm)	
	Sum	Maximum Daily
2015	686	66
2016	322	34
2017	525	47
2018	593	100
2019	766	97
2020	463	32

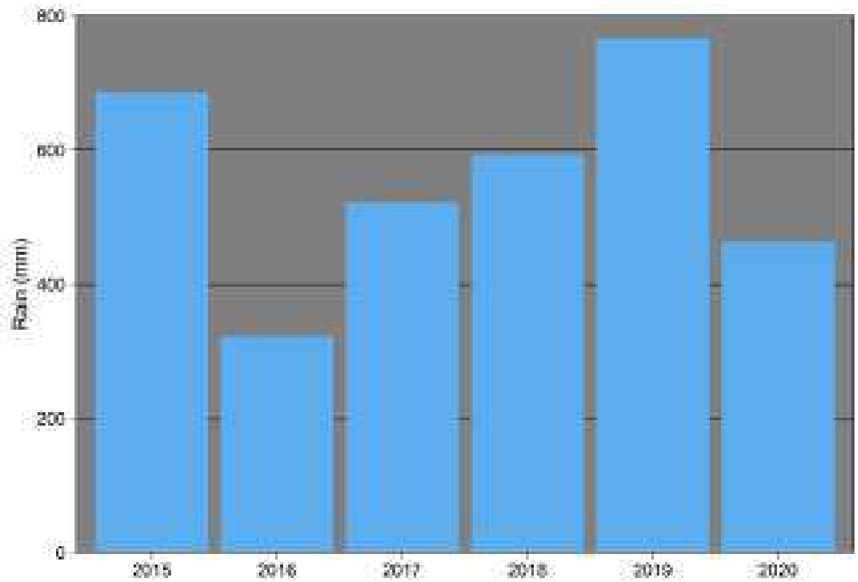

Figure 8. Annual cumulative rain depth between the years 2015-2020.

No substantial differences were found in the mean reference evapotranspiration (ET_o) values from 2015 to 2020, with ET_o ranging just 0.09 mm/d from 2.63 to 2.72 mm/d (Table 8; Figure 9). However, the annual evaporative atmospheric demands, were found to differ by up to 79 mm between 2015 and 2020, indicating that even a subtle increase in daily demands results in a remarkable annual increase. As in the case of air temperature, a slight upward trend is observed in the evaporative demands of the atmosphere between 2015-2020.

Table 8. Annual mean (in mm/day) and total reference evapotranspiration (in mm) between 2015-2020 in the Greek study area.

Year	Reference Evapotranspiration	
	Mean (mm/day)	Total (mm)
2015	2.63	857
2016	2.67	909
2017	2.66	872
2018	2.70	931
2019	2.71	895
2020	2.72	936

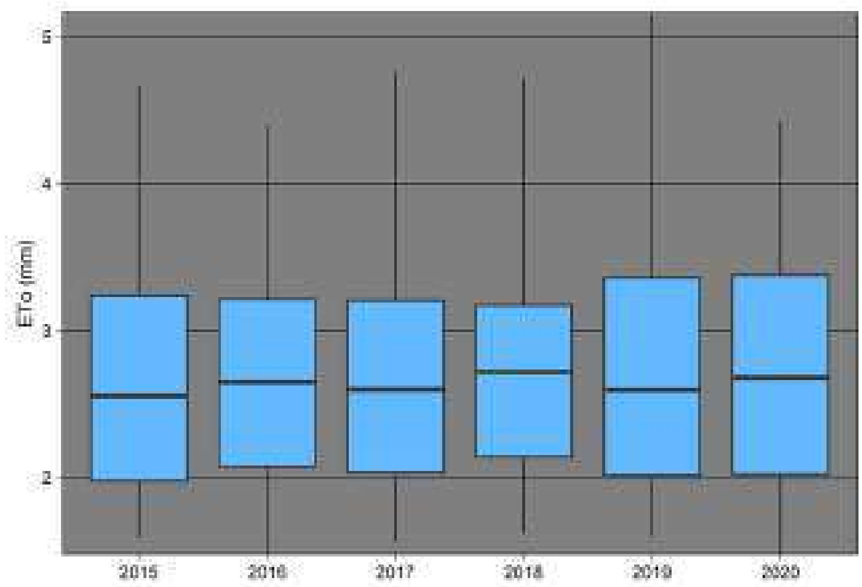

Figure 9. Annual reference evapotranspiration (ET_o) box charts between 2015-2020.

2.2 Copernicus Sentinel 2 mission imagery

The Copernicus Sentinel-2 mission comprises a constellation of two polar-orbiting satellites placed in the same sun-synchronous orbit, phased at 180° to each other. It aims at monitoring variability in land surface conditions, and its wide swath width (290 km) and high revisit time (10 days at the equator with one satellite, and 5 days with 2 satellites under cloud-free conditions, which results in 2-3 days at mid-latitudes) will support monitoring of Earth's surface changes. Sentinel-2 satellites are on track from 2015 to today and image data files consist of twelve spectral bands with maximum resolution of 10 m (Table 9).

Table 9. Spectral bands, central wavelengths (nm) and corresponding spatial resolutions (m) of Sentinel-2 MSI sensor.

Bands	**Central wavelength (nm)**	**Spatial Resolution (m)**
Band 1 (Coastal aerosol)	443	60
Band 2 (Blue)	490	10
Band 3 (Green)	560	10
Band 4 (Red)	665	10
Band 5 (Red Edge 1)	705	20
Band 6 (Red Edge 2)	740	20
Band 7 (Red Edge 3)	783	20
Band 8 (NIR)	842	10
Band 8A (NIR Vapor)	865	20
Band 9 (Water Vapor)	945	60
Band 10 (SWIR-Cirrus)	1375	60
Band 11 (SWIR-1)	1.610	20
Band 12 (SWIR-2)	2190	20

The required satellite imagery for this study was acquired via the R programming language, and more specifically the sen2r package (Ranghetti et al., 2020). To use the package, users must initially create (or already have) an account on Sentinel Scientific Data Hub (https://scihub.copernicus.eu/). In brief, through the sen2r user interface, users must initially provide their log-in credentials for the Sentinel Scientific Data Hub account and then define the borders of the study area, the desired sensing time interval, and the targeted vegetation indices. When executed, sen2r connects to the Sentinel Scientific Data Hub, searches for the available Level-1C (Top of the Atmosphere) products (for the given area and time), downloads them and subsequently process them with the European Space Agency snap toolbox to transform them to Level-2A (Bottom of the Atmosphere) products. Finally, it uses the products' bands to produce the targeted vegetation index maps.

The Sentinel tile that was found to be more suitable for the current work was T35TLF. The borders of the tile and the study area are depicted in Figure 10.

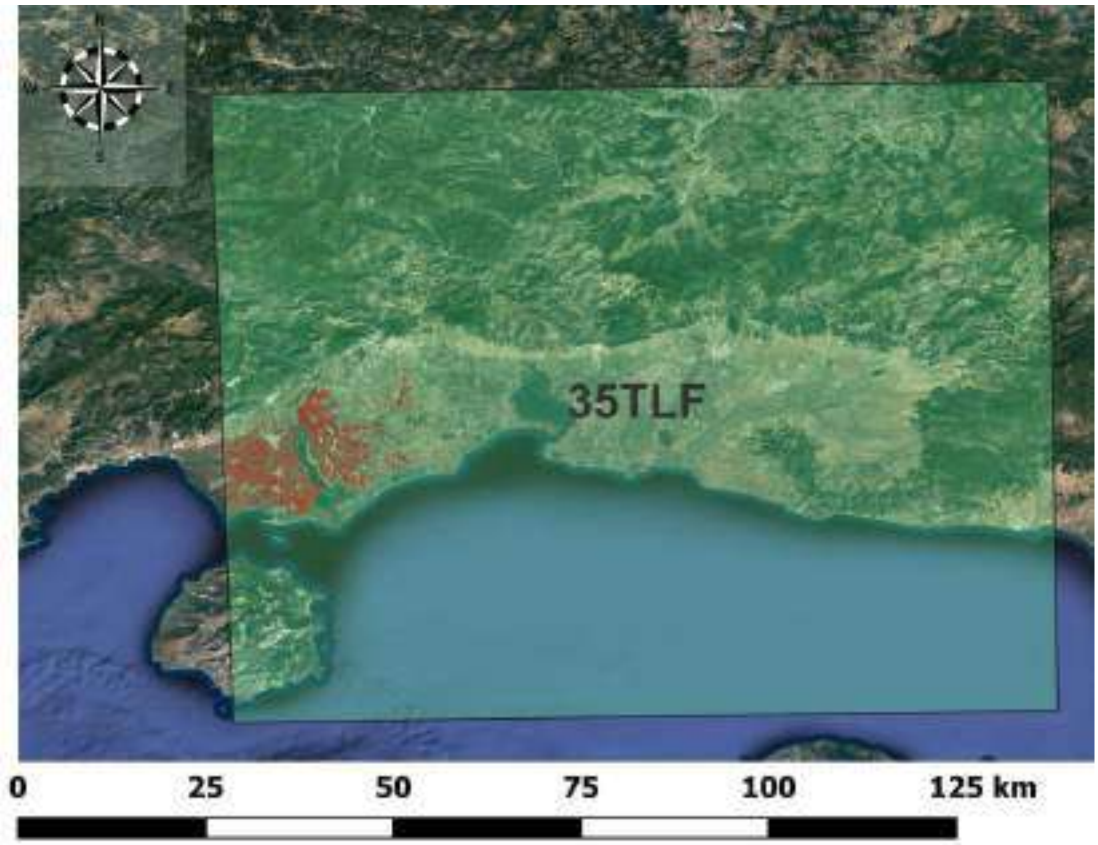

Figure 10. Sentinel 2 35TLF tile and study area fields.

In the case of the current study the selected vegetation index was NDVI, defined as the difference between the surface reflectance in near infrared and red wavelengths divided by the sum of surface reflectance in near infrared and red wavelengths. Thus, sen2r tool calculated NDVI using the Sentinel 2 spectral bands 4 (red) and 8 (near infrared) (Table 9) via the equation:

$$NDVI = \frac{NIR - RED}{NIR + RED} = \frac{Band8 - Band4}{Band8 + Band4} \quad (1)$$

NDVI index ranges between -1 to +1. Values lower than zero correspond to areas without any green vegetation, such as urban areas, bare rocks, areas covered with snow or waterbodies (e.g., oceans, lakes, rivers, etc.). Landscapes with NDVI values ranging from 0 to 0.3 are places with green vegetation of lower density, while surfaces with NDVI equal to 0.45 or higher correspond to areas occupied by dense to very dense green vegetation (Table 10) (Zaitunah et al., 2018).

Table 10. NDVI values for various vegetation cover.

Class	Dense Class	NDVI
1	Non Vegetation	< 0
2	Lowest Dense	0-0.15
3	Lower Dense	0.15-0.3
4	Dense	0.3-0.45
5	Higher Dense	0.45-0.6
6	Highest Dense	> 0.6

The total number of satellite images for the three years was 219, representing approximately 73 images per year. Initially the maximum allowed cloud cover was set to 0-2% and only 56 images were found to meet the criterion, resulting in an efficiency level equal to 26% (Table 11). The efficiency was slightly higher in 2020 (29%) than 2019 and 2018. When the allowed cloud cover was increased to 0-5% and 0-10%, the products that met the threshold increased to 72 and 87, respectively, thus substantially improving the efficiency level to 33% and 40%, respectively. Overall, the satellite images in year 2020 appeared more efficient than those in 2018 and 2019.

It is noteworthy that between March and June, for all years, a significant number of products were found to have a maximum cloud cover, higher than 10%. This is the time when the spring arable crops germinate and start to grow rapidly until they reach their maximum canopy cover, roughly to mid-June. This fact indicates that prolonged periods of cloud presence at certain periods of time may decrease the capacity of satellites to provide reliable services to agriculture.

Table 11. Sentinel 2 products acquired for the years 2018, 2019 and 2020.

Year	Total available	Cloud cover					
		0-2%	Eff. (%)	0-5%	Eff. (%)	0-10%	Eff. (%)
2018	73	19	26.03	22	30.14	25	34.25
2019	73	16	21.92	23	31.51	29	39.73
2020	73	21	28.77	27	36.99	33	45.21
Aggregate	219	56	25.57	72	32.88	87	39.73

2.2.1 Converting NDVI to CC

In order to convert the NDVI maps obtained from sen2r to CC maps, empirical equations proposed by previous studies were used. For all crops, the relationship between NDVI and CC was found to be linear, following the general form y = ax +b. Table 12 presents the equations used for each crop.

Table 12. Relationship between green canopy cover and NDVI for maize, cotton and rice crops.

Study	Crop	Equation
(Tsakmakis et al., 2021b)	Maize	$CC = 125 \times NDVI - 23.750$
(Sui et al., 2008)	Cotton	$CC = 0.69 \times NDVI + 16.52$
(Veerakachen and Raksapatcharawong, 2020)	Rice	$CC = 1.522 \times NDVI - 0.2457$

2.3 Irrigation Schedules

2.3.1 Farmers average irrigation schedules

To assess the amount of water that was applied typically during the cultivation period to maize and cotton crops in the study area, a number of interviews were conducted with farmers to better understand their philosophy and irrigation criteria. Based on the analysis of the questionnaires, an average irrigation schedule was created for maize and cotton.

In the case of maize, if no rainfall events occur during late March to early April, farmers irrigate after sowing to guarantee a successful germination. Subsequently, they let the maize plants grow and start to irrigate from the last week of May until crop maturation. The application frequency and amounts for furrow and drip irrigation systems (among the most popular in the area) are presented in Table 13.

Accordingly, if no rainfall events occur in April, farmers irrigate the cotton fields on sowing. Then, irrigation may be applied in the first half of June, if there are no rainfall events, but the plants are irrigated from late June to the end of August.

Table 13. Irrigation applications and frequency for the various irrigation systems in the case of maize and cotton crops.

Crop	Irri. System	Amount Applied per event (mm)	Frequency
Maize	Furrow	60	Every 4 days*
Maize	Drip	40	Every 4 days*
Cotton	Furrow	60	Every 5 days**
Cotton	Sprinkler	35	Every 5 days**
*From late May to maturity **From mid-June to maturity			

In the case of rice, the interviews with the farmers did not reveal any measurable data that can be used to create average irrigation schedules. In brief, from June to September, farmers open the gate barriers of the irrigation canal and let the water flood their fields on an almost daily basis. As long as the irrigated water amounts are not measured, it is almost impossible to create any irrigation scenario in the case of rice.

2.3.2 Optimum irrigation scenarios

Successively, aiming to obtain the optimum irrigation schedule for each experimental year, irrigation generation criteria were created for the targeted crops. For maize, the maximum plant available water depletion triggering an irrigation event was set to 50% of the total plant available water (TPAW) and the application amount was set equal to the amount required to bring soil back to FC (Table 14).

Table 14. Threshold criteria and application amounts defined for the optimum irrigation generation schedules.

Crop	Depletion (%)	Application Amount (mm)	Period
Maize	50	Back to FC	End of May to Maturity

2.3.3 National legislation irrigation water quotas evaluation

Both the farmer average empirical irrigation schedules, as well as the optimum derived irrigation schedules were used as means to assess the water quotas defined for the maize, cotton and rice crops by the 2nd Update of river basin management plans for the river basin district of Thrace (EL12) (Table 15). In brief, the water management plan defines that the maximum net water amount that can be applied to maize, cotton and rice equals to 5,562, 3,918 and 10,149 m^3/ha.

Table 15. Irrigation water quotas per crop in water district EL12 according to the 2nd Update of river basin management plans for river basin district (EL12) Thrace.

Crop Categories According to Crop Coefficient K	Crops	Net Total Water Quota During Cultivation Period (m^3/ha)	Allowed Irrigation Consumption from a Groundwell		
			MC (m^3/ha) via a drip irrigation system PC=85.50%	MC (m^3/ha) via a sprinkler irrigation system PC=80.75%	MC (m^3/ha) via a furrow irrigation system PC=50.00%
I K=0.55	Citrus Olives Vineyards	4,756 3,995 4,756	5,560 4,670 5,560		
II	Tobacco	3,419		4,230	

K=0.6					
III K=0.65	Cotton	3,918		4,850	
	Legumes	4,640		5,750	
	Orchards	5,208	6,090		
IV K=0.7	Sugar beets	5,656		7,000	
	Sunflower	5,656		7,000	
	Vegetables	6,133		7,590	
	Process Tomato	4,511		5,590	
	Potatoes	4,671		5,780	
	Melon fields	5,135		6,360	
V K=0.75	Winter Cereals	895		1,110	
	Maize	5,562		6,890	
VI K=0,80	Constructed Grasslands	3,507		4,340	
VII K=0,85	Alfalfa	7,510		9,300	
VIII K=1.2	Rice	10,149			20,300
MC=Maximum Consumption; PC=Irrigation System Performance Coefficient					

2.4 AquaCrop Model

AquaCrop (v 6.1) (Hsiao et al., 2009; Raes et al., 2009) is a crop growth model capable of simulating the growing cycle of grains, vegetables, tuber crops, cotton, maize etc. Its' function is partially based on the double crop coefficient concept (Allen et al., 1998), but it also incorporates the relatively novel concept of water productivity (WP*) in order to convert the plants' estimated transpiration to accumulative biomass (Steduto et al., 2007). The daily transpiration is calculated via the equation:

$$Tr_{Cadj} = K_S \times CC^* \times Kc_{Tr,x} \times ET_0 \tag{2}$$

where: K_S is the dimensionless soil water stress coefficient (equal to 1 when the soil is at field capacity and 0 at permanent wilting point); $Kc_{Tr,x}$ is the maximum crop transpiration coefficient (mm); ET_0 is the reference evapotranspiration (mm); and CC* is the canopy cover (%) adjusted for micro-advective effects given by the equation:

$$CC^* = 1.72CC - CC^2 + 0.30CC^3 \tag{3}$$

The dB accumulation in calculated in daily basis as:

$$dB = WP^* \times \sum_{i=1}^{n} \frac{Tr_{Cadj}}{ET_0} \tag{4}$$

where: dB is the accumulated dry aboveground biomass in day after sowing (DAS) n (tn/ha/d); and WP* is the crop's water productivity adjusted for atmospheric CO2 concentration and climate (g/m^2).

Finally, the model calculates the crop yield as:

$$Yield = HI \times B \quad (5)$$

where: Y is the crop production (tn/ha); and HI is the harvest index (%).

A deficit irrigation strategy may substantially enhance the water productivity of cotton (Fereres and Soriano, 2007). In AquaCrop this aspect is integrated with three intuitive parameters; a) the positive water stress impact on the HI when applied before flowering, b) the potentially positive effect of water stress on leaf expansion and in turn on HI during yield formation, and b) the potentially adverse effect of water stress induced stomatal closure on HI during yield formation. Thus, a decrease in dB production due to a deficit irrigation schedule may be compensated by an increase in HI resulting in increased water productivity.

At the current version 6.1, CC is a model output parameter. Its' growth and decline pattern over the growing cycle is calculated through the adjustment of input parameters a) canopy growth coefficient (CGC); b) canopy decline coefficient (CDC); c) maximum canopy cover (CC_x); and d) GDDs to senescence. In brief, after plants emergence and until $CC_x/2$ is reached, CC is calculated daily by the exponential function:

$$CC = CC_o e^{DAS \times CGC} \quad (6)$$

while from $CC_x/2$ to CC_x via the equation

$$CC = CC_x - 0.25 \frac{CC_x^2}{CC_o} e^{-DAS \times CGC} \quad (7)$$

For the time interval between CC_x is achieved until the beginning of the senescence stage, the CC is considered to remain constant. Then, the CDC was applied and the daily CC decline until the end of the season is estimated. A water shortage during CC development may result in limited or no CC development, a process simulated by the model through the water stress expansion coefficient. Similarly, a severe water shortage in the mid-season may trigger early CC senescence, a process estimated by the model through the corresponding senescence water stress coefficient.

The required input data for model execution are (a) a meteorological file; (b) a crop file; (c) a soil file; (d) an irrigation file; (e) a field management; (f) a groundwater file; and (g) an initial conditions file. In the framework of this work the meteorological, soil and irrigation files for each of the study area fields were created according to the collected data, as described in the respective subsections. The initial soil water content was considered to be close to FC and thus the upper 10 cm soil layer was adjusted to 90% of FC. This decision is justified by the rainfall events and the occurrence of low temperature prevailing in the study areas during March and early April. The field management and groundwater files were not used, as the groundwater table in all fields was below 40 m depth, whilst no mulching nor bounds were used as typical maize cultivation practices.

2.5 Water Footprint

According to the definitions and the methodological framework introduced by Hoesktra et al. (2011), the green and blue components of crop water requirements (CWR) are calculated by the accumulated data on daily crop evapotranspiration ET_c (mm/day), over the complete growing period, as follows:

$$CWR_{green} = 10 \times \sum_{d=1}^{lp} ET_{green} \tag{8}$$

$$CWR_{blue} = 10 \times \sum_{d=1}^{lp} ET_{blue} \tag{9}$$

where: CWR_{green} and CWR_{blue} are the green and blue component of crop water requirements (m3/ha), respectively; ET_{green} represents the rainwater lost by evapotranspiration (green water) (mm/d); and ET_{blue} the irrigated water lost by evapotranspiration (blue water) (mm/d) during the cultivation period. The summation is done over the period from the planting day (d=1) to the day of harvest (d=lp; lp is the length of growing period in days).

The ET_{green} and ET_{blue} evapotranspiration fractions were estimated in this study in two different ways. In the first approach (Hoekstra et al. 2011) the two models were executed initially under rainfed conditions. The cumulative ET_{Cadj} at the end of the season was considered equal to ET_{green}. Then, the models were run again under the ten different irrigation management scenarios (Table 1). For each scenario the ET_{blue} was calculated as:

$$ET_{blue} = ET_{Cadj\,i} - ET_{green} \qquad i = 1, 2, 3..., 10 \tag{10}$$

The green component of water footprint for growing a crop ($WF_{crop,green}$, m^3/tn) is calculated as the green component in crop water requirements (CWR_{green}, m^3/ha) divided by the crop yield (Y, tn/ha). Similarly, the blue component of water footprint ($WF_{crop,blue}$, m^3/tn) is defined as the ratio of the blue component in crop water requirements (CWR_{blue}, m^3/ha) against crop yield:

$$WF_{crop,green} = \frac{CWR_{green}}{Y} \tag{11}$$

$$WF_{crop,\mathrm{blue}} = \frac{CWR_{blue}}{Y} \tag{12}$$

For the calculations in above equations and in the case of the irrigation management scenarios 4, 5, 9 and 10, the experimentally measured seed cotton yield values were utilized, while for the rest of the scenarios the corresponding simulated by AquaCrop final seed cotton yields were used.

The water footprint of the process of growing crops or trees (WF_{crop}, m^3/tn) is the sum of the green and blue components:

$$WF_{crop} = WF_{crop,green} + WF_{crop,blue} \tag{13}$$

In a different perspective Chukalla et al. (2015) considered that the total soil water content (S) is the sum of a green component (Sg) and a blue component (Sb). The former one originated from rainfall water while the latter from irrigated water. Assuming that at the sowing date S has a specific composition i.e. 60% Sg and 40% Sb the daily changes in the two components until the end of the season are given by the following equations:

$$\frac{dSg}{dt} = R - \left(Dr + ET_{Cadj}\right)\left(\frac{Sg}{S}\right) - RO\left(\frac{R}{I+R}\right) \tag{14}$$

$$\frac{dSb}{dt} = I - \left(Dr + ET_{Cadj}\right)\left(\frac{Sb}{S}\right) - RO\left(\frac{I}{I+R}\right) \tag{15}$$

where: dt is the time step of the calculation (1d); R is the rainfall (mm); I is the irrigation (mm); Dr is the deep percolation (mm); and RO is the surface run off (mm). Subsequently, the daily ET_{green} and ET_{blue} values are calculated as follows:

$$ET_{green} = ET_{Cadj}\left(\frac{Sg}{S}\right) \tag{16}$$

$$ET_{blue} = ET_{Cadj}\left(\frac{Sb}{S}\right) \tag{17}$$

Then the equations (11) and (12) – (13) are used again to estimate the green, blue and total cotton water footprint, respectively.

In the current study, S at the sowing day was assumed to be equal to Sg as all available soil water at the beginning of the cultivation season comes from the winter and early spring rainfalls.

3 Results and Discussion

3.1 Variations of soil hydraulic properties

When the gravel content was set equal to zero and the compaction level to normal, the soil data analysis results showed that soil FC mean value was considerably higher for clay loam fields (33.18% in average), whilst the lowest mean value (18.77%) was calculated for fields characterized as sandy loams (Table 16). The standard deviation for all textural classes exhibited very similar values, ranging from 1.93% to 2.78%. Moreover, the largest number of outlier fields, meaning that these fields showed FC values outside the box plot whiskers specially to the lower end, was observed in the case of sandy loam textural class (Figure 11). Specifically, while the mean FC value was found to be roughly 19%, the minimum calculated FC within the textural class was just 10%.

Similarly, the PWP mean value was higher for clay loam fields and lower for sandy loams taking values equal to 19.81% and 8.46%, respectively (Table 17). Standard deviation showed slightly lower values than those in FC, ranging between 1.61% and 2.17%. Again, the largest number of outliers were observed in the case of sandy loam fields, showing minimum value equal to just 2.76%.

Defined as the difference between FC and PWP, the plant available water (paw) was found to take larger values for loam and clay loam fields than at the sandy clay loam and sandy loam fields (Figure 11). In detail, the mean paw for loams and clay loams was roughly 132 mm of water per meter of soil, while this amount was considerably lower in the case of sandy loams and sandy clay loams, equal to approximately 100 mm (Table 18). The minimum and maximum paw values were estimated for sandy loam and loam fields, equal to 60 mm and 169 mm, respectively. These results indicate that the paw values of cultivated fields should be taken into consideration during the irrigation scheduling process, especially for the fields that belong to the upper or lower extreme cases, as otherwise an irrational use of the available water resources is very likely to happen.

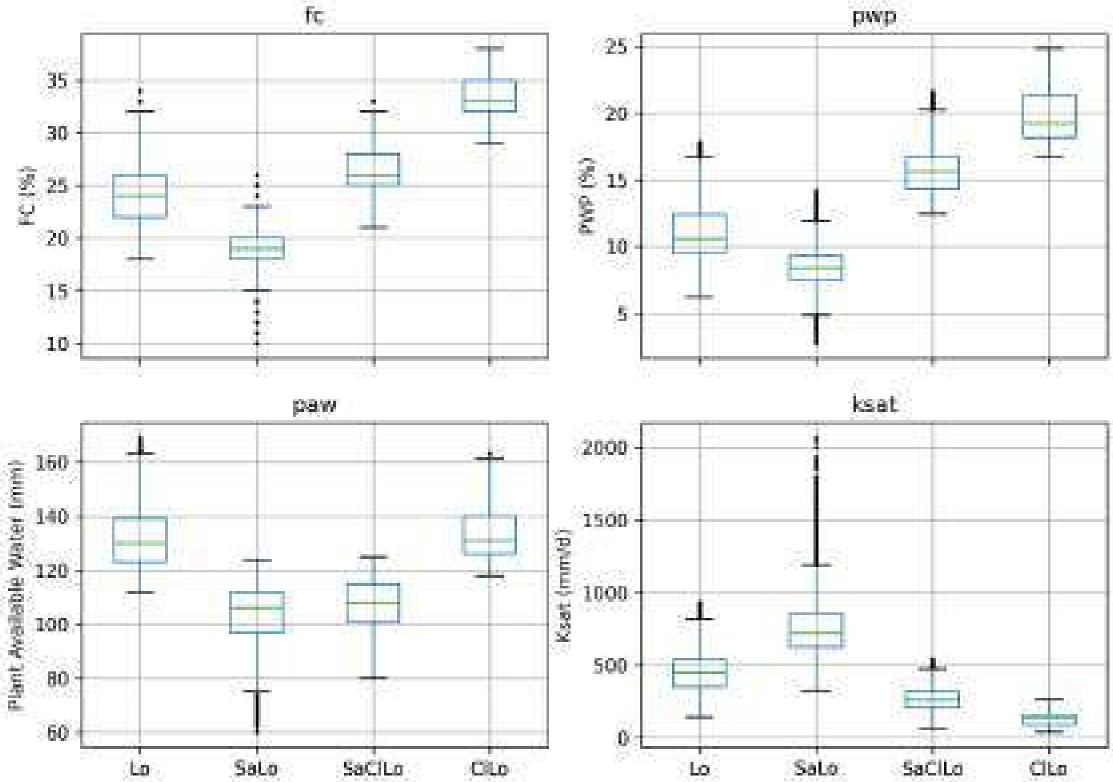

Figure 11. Variations of fields capacity (FC), permanent wilting point (PWP), plant available water (paw) and saturated hydraulic conductivity (K_{sat}) in the case of Loam (Lo), Sandy Loam (SaLo), ClayLoam (ClLo) and Sandy Clay Loam (SaClLo) textural classes. Gravel content = 0; Compaction Level = Normal.

Saturated hydraulic conductivity analysis showed that clay loam fields are more difficult to drain, taking a mean value equal to 126 mm/d, but within the same class fields with K_{sat} of just 37 mm/d were also present (Table 19). It is obvious that by applying an excess of water in the later fields, runoff of stagnation phenomena is very likely to occur, resulting in a loss of water via a nonproductive way (e.g., evaporation). On the other hand, extremely high K_{sat} values were observed in the case of sandy loam fields, larger than 2,000 mm/d. While an application of excess water will have the same result as in the case of clay loam fields, an irrational use of water resources, however the loss mechanism for sandy loam soils is deep percolation, meaning that the applied water infiltrates deeper than plants' rooting depth and is being lost to groundwater. Loams and sandy clay loams showed a moderate drainage ability, showing K_{sat} mean values 447 mm/d and 260 mm/d, respectively.

Table 16. Statistics of the textural class impact on soil field capacity (%).

	Lo	SaLo	SaClLo	ClLo
count	14238	13879	2834	1027
mean	24.33	18.77	26.52	33.18
std	2.78	2.25	2.39	1.93
min	18	10	21	29
25%	22	18	25	32
50%	24	19	26	33
75%	26	20	28	35
max	34	26	33	38
Lo=Loam; SaLo=Sandy Loam; ClLo=Clay Loam; SaClLo=Sandy Clay Lom; std=Standard Deviation				

Table 17. Statistics of the textural class impact on soil permanent wilting point (PWP) (%).

	Lo	SaLo	SaClLo	ClLo
count	14238	13879	2834	1027
mean	11.14	8.46	15.76	19.81
std	2.17	1.61	1.82	2.01
min	6.25	2.76	12.46	16.7
25%	9.56	7.5	14.34	18.18
50%	10.56	8.39	15.61	19.23
75%	12.42	9.27	16.72	21.3
max	17.81	14.19	21.58	24.83
Lo=Loam; SaLo=Sandy Loam; ClLo=Clay Loam; SaClLo=Sandy Clay Lom; std=Standard Deviation				

Table 18. Statistics of the textural class impact on soil plant available water (mm).

	Lo	SaLo	SaClLo	ClLo
count	14238	13879	2834	1027
mean	131.84	103.17	107.64	133.81
std	10.56	11.16	8.73	9.95
min	112	60	80	118
25%	123	97	101	126
50%	130	106	108	131
75%	139	112	115	140
max	169	124	125	163
Lo=Loam; SaLo=Sandy Loam; ClLo=Clay Loam; SaClLo=Sandy Clay Lom				

Table 19. Statistics of the textural class impact on saturated hydraulic conductivity (mm/d).

	Lo	SaLo	SaClLo	ClLo
count	14238	13879	2834	1027
mean	446.76	760.05	259.11	125.57
std	127.66	210.95	80.91	43.54
min	142.41	323.38	63.56	36.59
25%	350.84	628.07	208.29	88.86
50%	450.54	721.72	260.26	132
75%	539.1	854.3	316.08	160.74
max	932.73	2066.96	539.04	264.05
Lo=Loam; SaLo=Sandy Loam; ClLo=Clay Loam; SaClLo=Sandy Clay Lom				

3.1.1 Impact of gravel content on plant available water

The parameters that are affected by the presence of gravels within the soil matrix are paw and K_{sat}. Increased gravel content reduces the number of the available pores and thus the volume that water can occupy per soil unit (e.g., water cm^3 / soil cm^3). As a result, the presence of gravels decreases the amount of water that a soil could withhold and thus the total paw. It should be mentioned that the FC and PWP parameters values are independent of gravel content and their values remain the same.

For all textural classes, the paw is reduced as the gravel content appears increased (Figure 12). The impact of gravels was found to be more profound in the case of clay loam and sandy clay loam textural classes. For these classes an increase of gravel content from 0% to 30%, resulted in a paw decrease equal to 25-28 mm of water, a reduction that corresponds to a decrease of roughly 20-23% (Tables 22, 23). On the other hand, in the case of loam and sandy loam the observed decrease was found to be moderately less fluctuating between 16-18% (16 -23 mm) (Table 20, 21).

In the extreme scenario of a soil with a gravel content equal to 60% loam and clay loam soil, a decrease in paw up to 60 mm of water was shown, whilst in the case of sandy loam and sandy clay loam fields this amount was considerably lower, equal to 50 mm. Overall, a gravel content equal to 60%, results in a paw reduction larger than 40% to all textural classes.

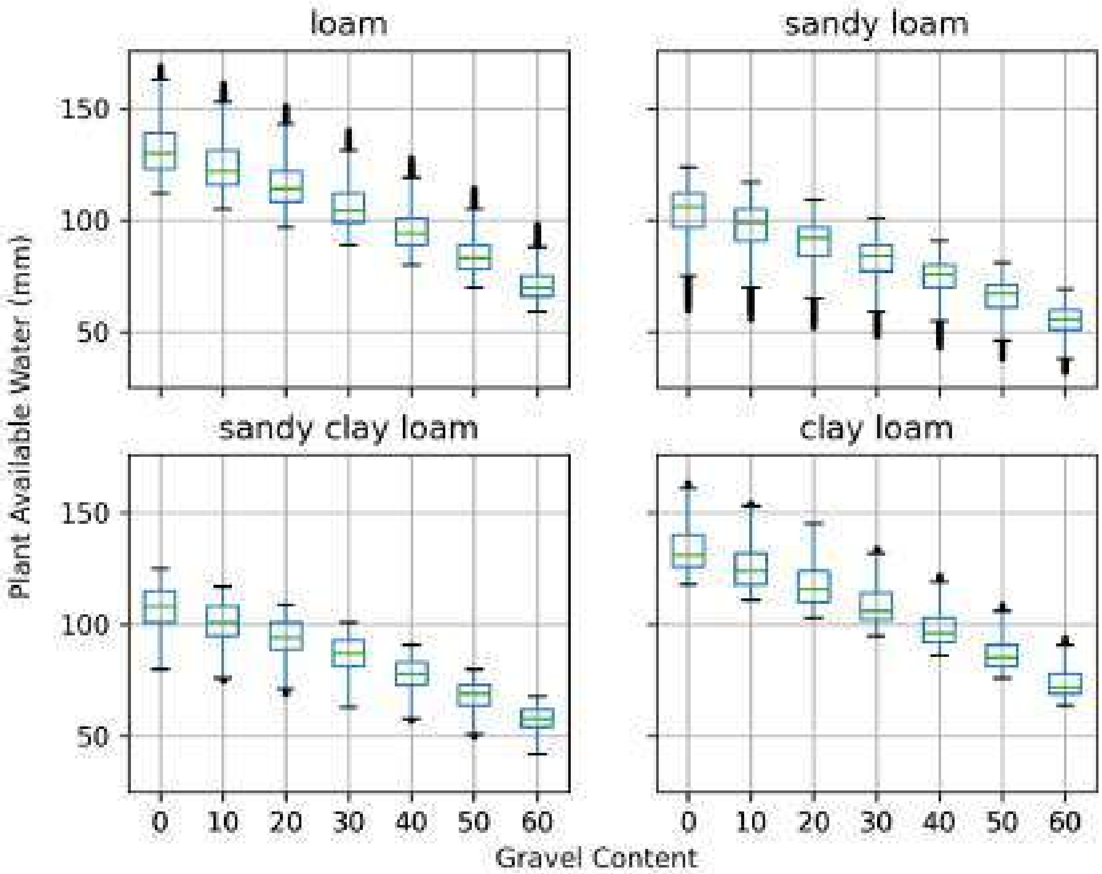

Figure 12. Impact of gravel content on plant available water for loam, sandy loam, sandy clay loam and clay loam textural classes.

Table 20. Statistics of the gravel content impact on total plant available water (mm) in the case of Loam textural class.

	0	10	20	30	40	50	60
count	14238	14238	14238	14238	14238	14238	14238
mean	131.84	124.02	115.45	106.03	95.63	84.09	71.2
std	10.56	10.08	9.54	8.93	8.21	7.39	6.41
min	112	105	97	89	80	70	59
25%	123	116	108	99	89	78	66
50%	130	122	114	104	94	83	70
75%	139	131	122	112	101	89	75
max	169	161	151	140	128	114	98

Table 21. Statistics of the gravel content impact on total plant available water (mm) in the case of Sandy Loam textural class.

	0	10	20	30	40	50	60
count	13879	13879	13879	13879	13879	13879	13879
mean	103.17	96.88	90.01	82.5	74.23	65.1	54.96
std	11.16	10.51	9.79	9	8.13	7.17	6.09
min	60	56	52	48	43	38	32
25%	97	91	84	77	70	61	51
50%	106	99	92	84	76	67	56
75%	112	105	97	89	80	71	60
max	124	117	109	101	91	81	69

Table 22. Statistics of the gravel content impact on total plant available water (mm) in the case of Sandy Clay Loam textural class.

	0	10	20	30	40	50	60
count	2834	2834	2834	2834	2834	2834	2834
mean	107.64	101.19	94.14	86.42	77.89	68.44	57.89
std	8.73	8.29	7.79	7.23	6.6	5.88	5.06
min	80	75	69	63	57	50	42
25%	101	95	89	81	73	64	54
50%	108	101	94	87	78	69	58
75%	115	108	101	93	83	73	62
max	125	117	109	101	91	80	68

Table 23. Statistics of the gravel content impact on total plant available water (mm) in the case of Clay Loam textural class.

	0	10	20	30	40	50	60
count	1027	1027	1027	1027	1027	1027	1027
mean	133.81	126.2	117.84	108.57	98.28	86.78	73.81
std	9.95	9.55	9.09	8.55	7.91	7.19	6.27
min	118	111	103	95	86	76	64
25%	126	118	110	102	92	81	69
50%	131	124	116	106	96	85	72
75%	140	132	124	114	103	91	78
max	163	154	145	134	122	109	94

3.1.2 Impact of gravel content to saturated hydraulic conductivity (K_{sat})

As in the case of the paw, the presence of gravels within the soil matrix decreases the available water infiltrate paths and thus results in the decrease of K_{sat}. For all the textural classes an increase of gravel content to 10%, 20%, 30%, 40%, 50% and 60% resulted in a K_{sat} decrease equal to approximately 8.5%, 9.5%, 10.5%, 12%, 13.6% and 16%, respectively (Figure 13). In terms of absolute numbers, the largest decrease was observed in the sandy loam fields in which the K_{sat} mean value plummeted from 760 mm/d in the case of 0% gravel content to 328 mm/d in 60% gravel content scenario, a decrease equal to 432 mm/d (Table 25). Despite this significant decrease, the K_{sat} of sandy clay soils remains remarkably high (even with the 60% gravel content), allowing them to infiltrate almost 14 mm of water per hour. Accordingly, loam fields maintain the ability to infiltrate large amounts of water (> 10 mm/hr) for gravel content values up to 50%, whilst at 60% their K_{sat} was found to marginally fall below 10 mm/hr.

On the contrary, in the case of clay loam fields, every 10% increase in the gravel content resulted in an approximate decrease of 0.5mm/hr in the already low K_{sat} mean value of 5 mm/hr at 0% gravel content. Ultimately, at 60% gravel content, these fields showed a K_{sat} of roughly 2 mm/hr (Table 27).

Sandy clay loam fields mean K_{sat} showed values lower than 10 mm/hr with just a 10% increase in gravel content (Table 26), resulting in 9.85 mm/hr and 7.89 mm/hr at 10% and 30% gravel content, respectively.

Overall, the statistical analysis showed that the presence of gravel content on clay loam and sandy clay loam fields affects even more the already challenging irrigation scheduling task in these fields. In detail, an irrigation schedule of frequent and small applications of water seems to be the ideal pattern, with the application amount being reduced as the gravel content increases.

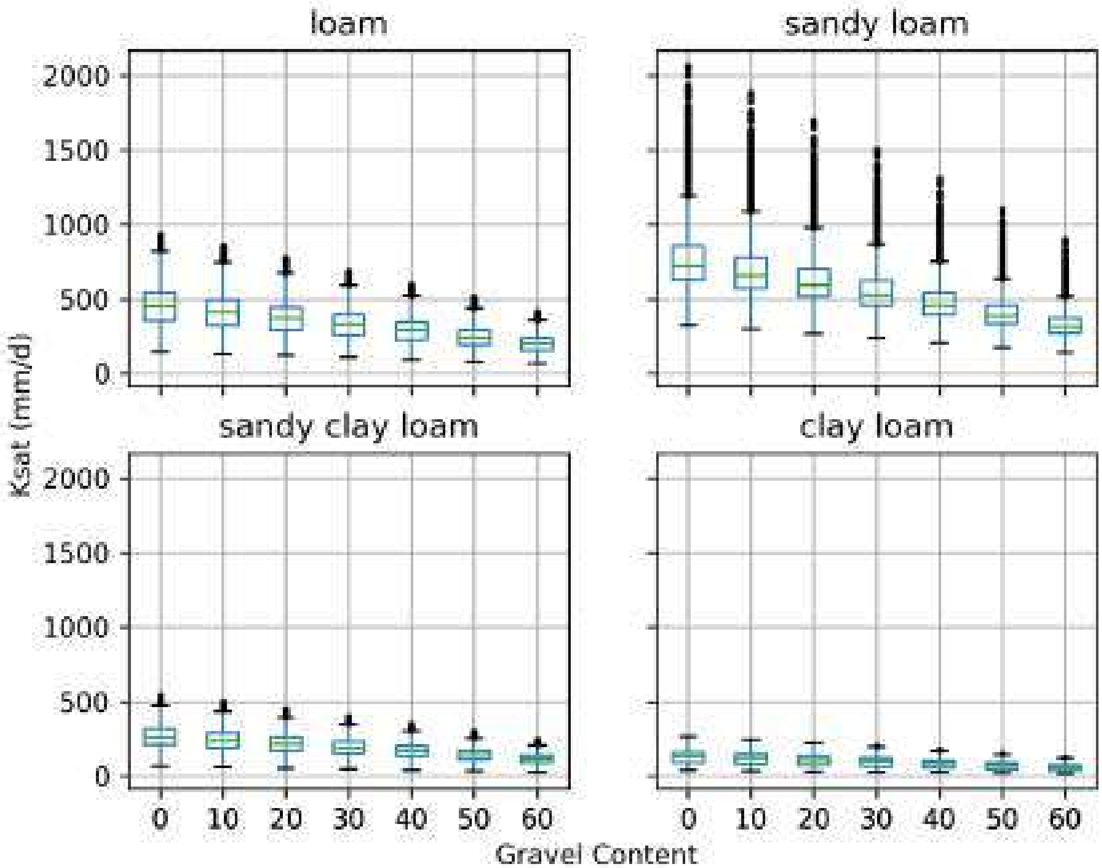

Figure 13. Impact of gravel content on saturated hydraulic conductivity (Ksat) for loam, sandy loam, sandy clay loam and clay loam textural classes.

Table 24. Statistics of the gravel content impact on saturated hydraulic conductivity in the case of Loam textural class.

	0	10	20	30	40	50	60
count	14238	14238	14238	14238	14238	14238	14238
mean	446.76	407.98	368.04	326.9	284.5	240.78	195.68
std	127.66	116.37	104.8	92.92	80.73	68.2	55.34
min	142.41	130.36	117.89	104.98	91.6	77.73	63.35
25%	350.84	320.62	289.47	257.46	224.31	190	154.63
50%	450.54	411.28	370.98	329.45	286.64	242.44	196.91
75%	539.1	492.12	443.66	393.78	342.46	289.59	235.18
max	932.73	853.47	771.53	686.75	598.99	508.09	413.88

Table 25. Statistics of the gravel content impact on saturated hydraulic conductivity in the case of Sandy Loam textural class.

	0	10	20	30	40	50	60
count	13879	13879	13879	13879	13879	13879	13879
mean	760.05	692.5	623.26	552.27	479.46	404.75	328.07
std	210.95	192.14	172.88	153.15	132.93	112.19	90.92
min	323.38	294.31	264.59	234.18	203.06	171.21	138.6
25%	628.07	572.4	514.83	456.07	395.77	334.02	270.73
50%	721.72	657.69	592	524.79	455.56	384.63	311.78
75%	854.3	778.64	700.99	621.08	539	454.94	368.63
max	2066.96	1884.78	1697.73	1505.62	1308.24	1105.37	896.77

Table 26. Statistics of the gravel content impact on saturated hydraulic conductivity in the case of Sandy Clay Loam textural class.

	0	10	20	30	40	50	60
count	2834	2834	2834	2834	2834	2834	2834
mean	259.11	236.48	213.2	189.25	164.6	139.22	113.06
std	80.91	73.78	66.46	58.95	51.23	43.29	35.13
min	63.56	57.97	52.22	46.32	40.25	34.01	27.6
25%	208.29	189.97	171.29	152.14	132.49	112.12	91.15
50%	260.26	237.55	214.11	190.12	165.32	139.95	113.65
75%	316.08	287.94	259.88	230.66	200.54	169.83	137.85
max	539.04	494.31	447.85	399.57	349.36	297.09	242.63

Table 27. Statistics of the gravel content impact on saturated hydraulic conductivity in the case of Clay Loam textural class.

	0	10	20	30	40	50	60
count	1027	1027	1027	1027	1027	1027	1027
mean	125.57	115.17	104.36	93.13	81.44	69.27	56.59
std	43.54	40.03	36.36	32.53	28.52	24.33	19.94
min	36.59	33.51	30.31	27	23.56	20	16.31
25%	88.86	81.38	73.66	65.78	57.57	49.05	40.17
50%	132	120.99	109.27	97.44	85.18	72.31	58.98
75%	160.74	147.36	133.66	119.26	104.3	88.74	72.5
max	264.05	243.99	222.83	200.48	176.83	151.76	125.15

3.1.3 Impact of field compaction on plant available water

Soil compaction occurs when soil particles are pressed together, reducing pore size between them. Specifically, compaction decreases the field's FC but leaves unaffected the PWP. As a result, the soil capability to withhold water is decreased, ultimately reducing the paw level (Figure 14).

The results showed that from normal to dense compaction level the paw was reduced 8.64%, 11.35%, 10.76% and 8.12% for loam, sandy loam, sandy clay loam and clay loam classes, respectively, while in the case of severe compaction level these percentages were found to be equal to 25.90%, 34.03%, 31.97% and 24.36%.

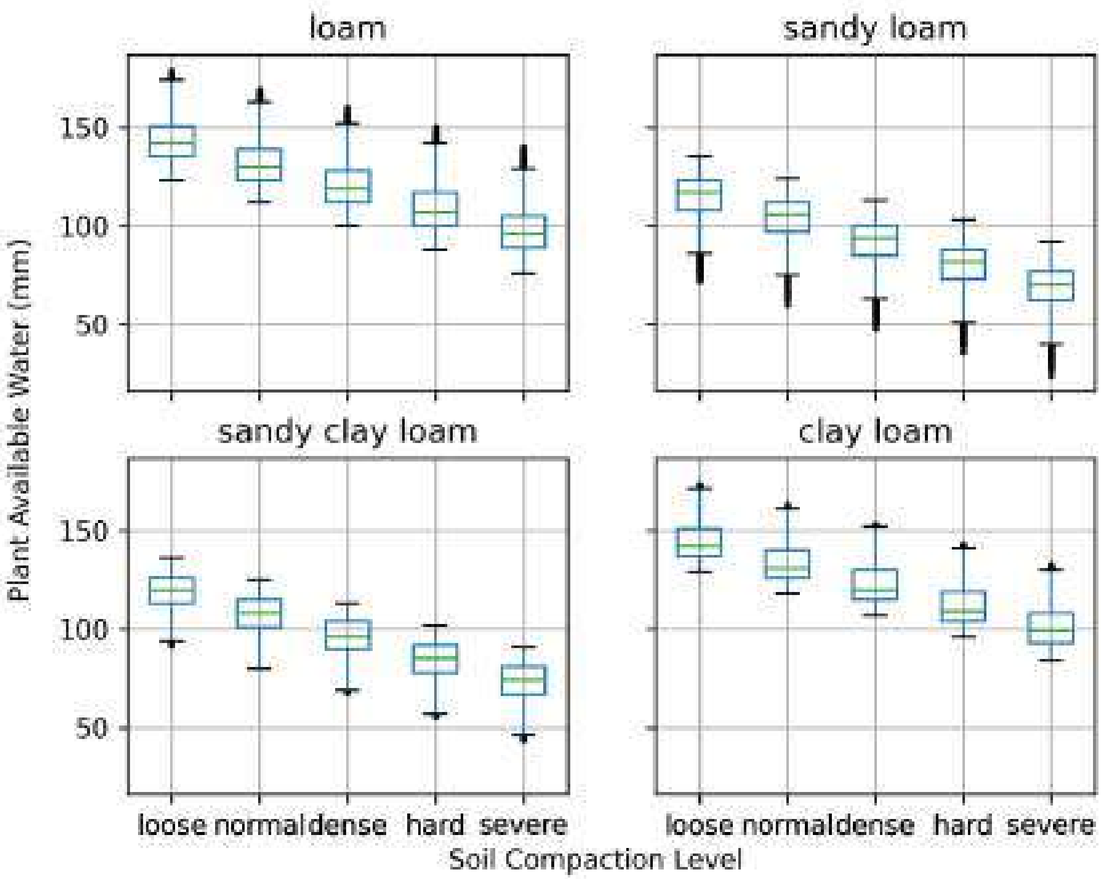

Figure 14. Impact of soil compaction level on plant available water for loam, sandy loam, sandy clay loam and clay loam textural classes.

In terms of paw (in mm) of water, all soil classes were gaining roughly 10 to 11 mm of water, when moving from normal towards the loose soil compaction level. On the other hand, from normal to dense, all four classes lost approximately 10 mm and then again, another 10 mm to hard and severe compaction levels, losing in total roughly 34 mm of water (Tables 28, 29, 30, 31).

Analysis results indicated that soil compaction is a factor that if not measured, increases the uncertainty of water balance model calculations, as it directly affects the soil maximum water holding capacity and thus paw, altering the optimum irrigation scheduling schema (both frequency and application amount).

Table 28. Statistics of the soil compaction level impact on plant available water in the case of Loam textural class.

	loose	normal	dense	hard	severe
count	14238	14238	14238	14238	14238
mean	143.23	131.84	120.47	109.09	97.7
std	10.35	10.56	10.78	11	11.23
min	123	112	100	88	76
25%	135	123	112	100	89
50%	142	130	119	107	96
75%	150.75	139	128	117	105
max	179	169	160	150	140

Table 29. Statistics of the soil compaction level impact on plant available water in the case of Sandy Loam textural class.

	loose	normal	dense	hard	severe
count	13879	13879	13879	13879	13879
mean	114.88	103.17	91.47	79.77	68.06
std	11.11	11.16	11.22	11.28	11.34
min	72	60	48	36	24
25%	108	97	85	73	62
50%	117	106	94	82	70
75%	123	112	100	88	77
max	135	124	113	103	92

Table 30. Statistics of the soil compaction level impact on plant available water in the case of Sandy Clay Loam textural class.

	loose	normal	dense	hard	severe
count	2834	2834	2834	2834	2834
mean	119.1	107.64	96.16	84.69	73.23
std	8.57	8.73	8.88	9.04	9.19
min	92	80	68	56	44
25%	113	101	90	78	67
50%	120	108	96	85	74
75%	126	115	104	92	81
max	136	125	113	102	91

Table 31. Statistics of the soil compaction level impact on plant available water in the case of Clay Loam textural class.

	loose	normal	dense	hard	severe
count	1027	1027	1027	1027	1027
mean	144.68	133.81	122.95	112.08	101.21
std	9.72	9.95	10.19	10.43	10.68
min	129	118	107	96	84
25%	137	126	115	104	93
50%	142	131	120	109	99
75%	151	140	130	119	108
max	173	163	153	143	133

3.1.4 Impact of field compaction on saturated hydraulic conductivity (K_{sat})

Beyond FC and subsequently paw, compaction affects K_{sat} (Figure 15). It is remarkable that loam, sandy clay loam and clay loam fields under severe compaction level can even be impenetrable (K_{sat} = 0 mm/d) (Tables 32, 34, 35). Clay loam and sandy clay loam fields with a compaction level hard or higher, cannot be cultivated, as their mean K_{sat} values 25 mm/d (1 mm/hr) and 6 mm/day (0.24 mm/d) renders their irrigation problematic. Similarly, loam fields with a severe compaction level do now allow sufficient water to infiltrate through their pores for irrigation purposes (K_{sat} = 0.6 mm/d), while targeted irrigation schedules (very low application rate) must be implemented in the case of hard compaction levels.

Despite the significant decrease in the mean K_{sat} value from normal to severe compaction level (roughly 93%), sandy loam fields can still allow up to 50 mm/d to infiltrate through their matrix under this adverse state (Table 33).

Overall, the lack of data regarding the field compaction level may lead to significant water balance miscalculations, specifically in the case of loam, sandy clay loam and clay loam fields, leading to false estimations and results.

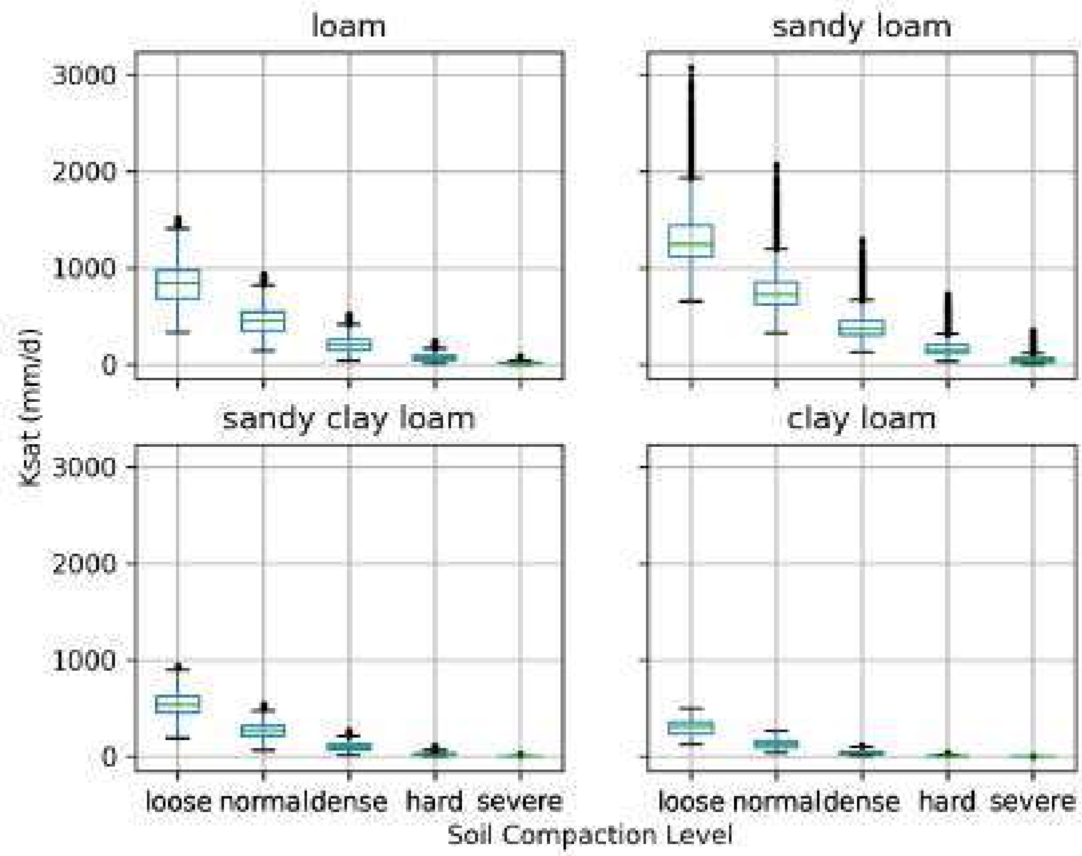

Figure 15. Impact of soil compaction level on saturated hydraulic conductivity for loam, sandy loam, sandy clay loam and clay loam textural classes.

Table 32. Statistics of the soil compaction level impact on saturated hydraulic conductivity (mm/d) in the case of Loam textural class.

	loose	normal	dense	hard	severe
count	14238	14238	14238	14238	14221
mean	826.29	446.76	204.34	70.27	13.53
std	198.13	127.66	73.6	35.11	11.38
min	331.43	142.41	42.12	4.88	0
25%	679.75	350.84	148.31	43.06	4.73
50%	837.89	450.54	203.48	67.41	11.03
75%	973.66	539.1	255.5	93.21	19.46
max	1513.42	932.73	518.6	246.64	90.55

Table 33. Statistics of the soil compaction level impact on saturated hydraulic conductivity (mm/d) in the case of Sandy Loam textural class.

	loose	normal	dense	hard	severe
count	13879	13879	13879	13879	13879
mean	1299.69	760.05	392.67	167.3	50.94
std	301.13	210.95	136.52	78.37	36.73
min	654.06	323.38	127.18	31.97	2.15
25%	1113.01	628.07	306.4	117.28	27.75
50%	1247.46	721.72	365.75	149.94	41.13
75%	1437.84	854.3	450.7	197.73	62.48
max	3075.81	2066.96	1292.8	731.61	356.87

Table 34. Statistics of the soil compaction level impact on saturated hydraulic conductivity (mm/d) in the case of Sandy Clay Loam textural class.

	loose	normal	dense	hard	severe
count	2834	2834	2834	2834	2497
mean	532.65	259.11	100.01	24.99	2.47
std	134.45	80.91	41.44	15.62	3
min	190.73	63.56	10.77	0.06	0
25%	449.54	208.29	72.71	13.73	0.59
50%	538.06	260.26	99.03	23.3	1.43
75%	628.8	316.08	128.36	34.5	3.42
max	934.81	539.04	273.3	112.85	31.82

Table 35. Statistics of the soil compaction level impact on saturated hydraulic conductivity (mm/d) in the case of Clay Loam textural class.

	loose	normal	dense	hard	severe
count	1027	1027	1027	1021	445
mean	293.6	125.57	38.32	5.66	0.22
std	77.03	43.54	19.52	5.22	0.62
min	125.37	36.59	4.22	0	0
25%	231.04	88.86	22.06	1.36	0
50%	308.24	132	38.99	4.67	0.05
75%	357.2	160.74	53.6	8.92	0.15
max	496.54	264.05	117.43	37.92	5.79

3.2 Satellite imagery NDVI data

3.2.1 Maize NDVI data

The development of the NDVI index and its distribution over the Nestos Delta fields, throughout the 2018, 2019 and 2020 cultivation seasons for maize crop is illustrated in Figures 16, 17 and 18, respectively. The maize seeds were sowed between March 20, 2018 to April 15, 2018 in the study area, and they usually germinate within 10 – 15 days from sowing. The plants grow slowly till mid-May and then their canopy grows rapidly to reach its maximum CC until June 15, 2018. From June 15, 2018 till August 10, 2018, the wealthy, adequately irrigated maize plants show NDVI values higher than 0.75.

In 2019 and 2020, when maize seeds were sowed in the first week of April, NDVI values remained lower than 0.4 in all fields till mid-May. This was due to the fact that the maize plants have just germinated, and their CC-values were very low. From May 15, 2019 and onwards, NDVI started to increase rapidly, showing on average values higher than 0.7 during June, July and August. In September, when the plants have been harvested, the NDVI values dropped again below 0.5.

It is noteworthy that in 2018, when the maize seeds were sowed on March 20, NDVI values close to 0.5 were observed from late April. Again, high NDVI values (> 0.7) were monitored during June and July, but in August the average NDVI was found to be moderately lower (< 0.6) than that of years 2019 and 2020 (~ 0.7), probably due to the fact that the plants sowed earlier and thus they reached maturation earlier this year.

Despite the general trend that was observed in the majority of fields throughout the studied period, there were cases in which the NDVI value of certain fields did not follow the general trend. For instance, there were fields with NDVI values lower than the mean, during the whole cultivation season, or in some specific development stage. It is hard to say if these low values are attributed to problematic irrigation, poor fertilization, pests' infection or some other reason, but it is clear that plants on these fields experienced stress, and thus their final yield will not be optimum.

One of the key growing stages with low NDVI values resulting in decreased maize yields is July, the period of maize kernel formation. Figure 19 shows the number of fields experiencing stress, i,e., exhibiting NDVI values lower than 0.7 on July 15, July 25 and July 14 in 2018, 2019 and 2020, respectively. Specifically, on July 15, 2018, 1,065 fields out of 8,254 (roughly 12.9%) were found to show NDVI values lower than 0.7. The number of stressed fields was considerably lower in 2019; they were equal to 706 out of 8,045 (8.76%), but increased again moderately in 2020, to reach 987 stressed fields out of 7.336 (13.5%).

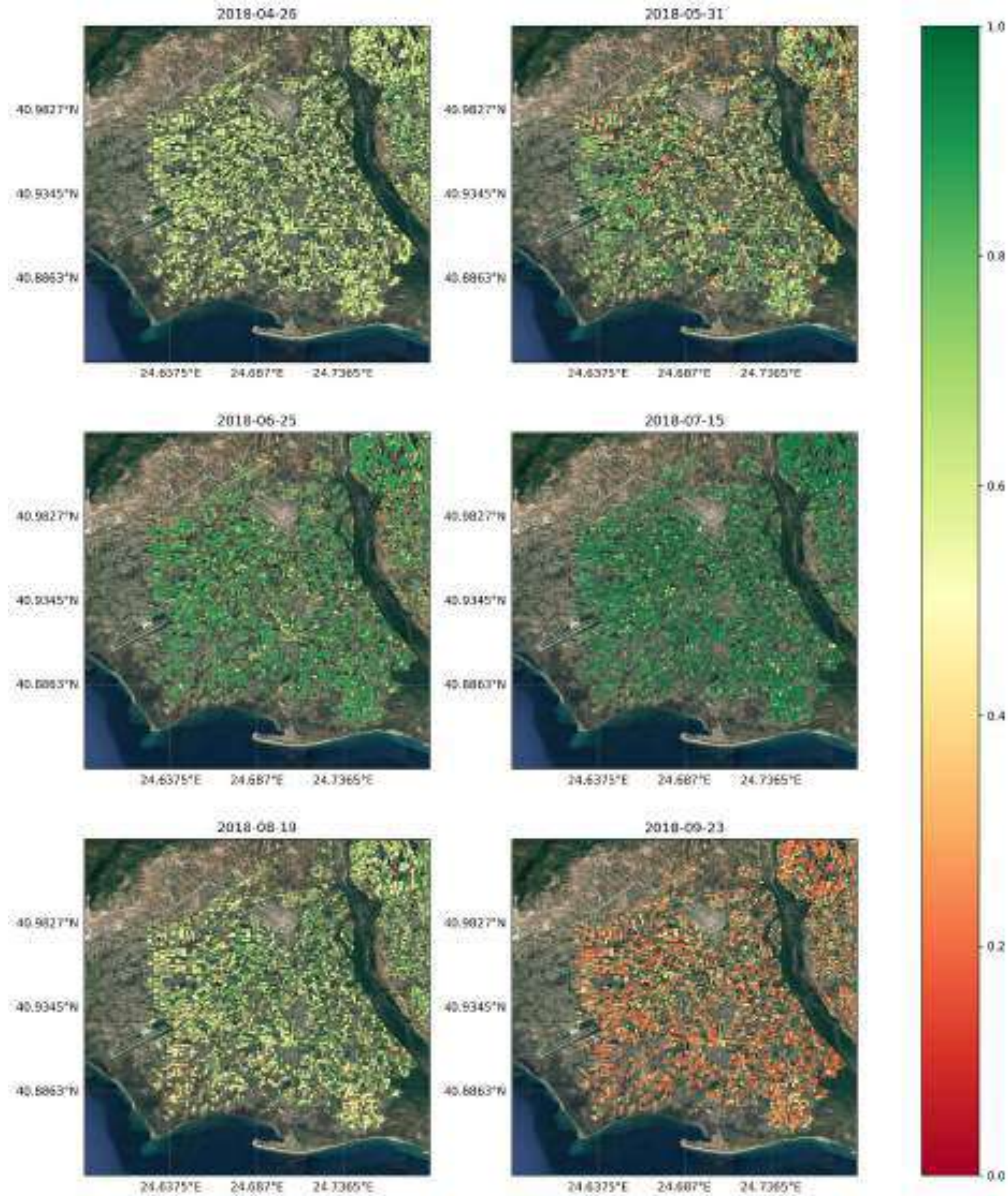

Figure 16. NDVI development through 2018 cultivation season for maize crop.

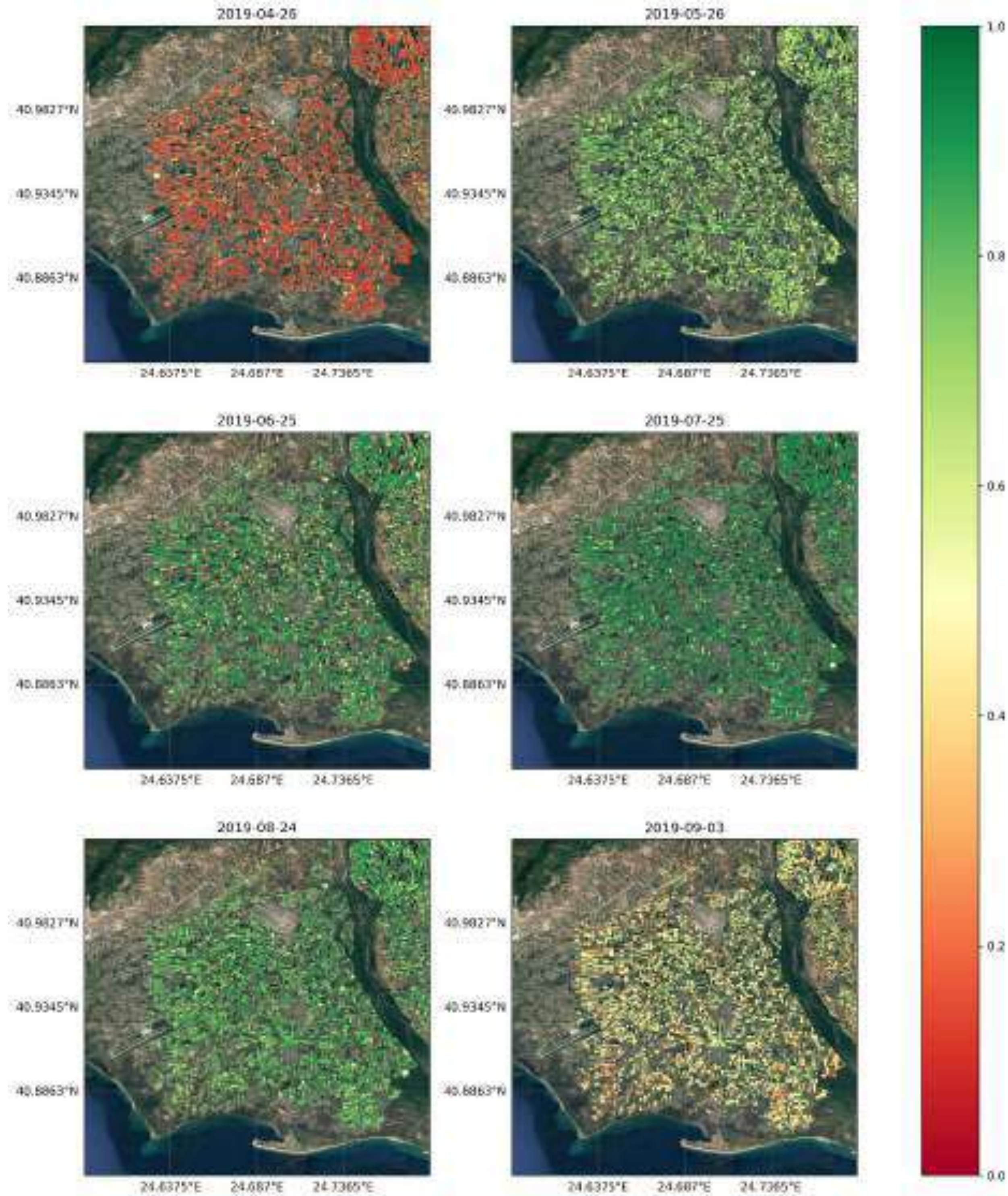

Figure 17. NDVI development through 2019 cultivation season for maize crop.

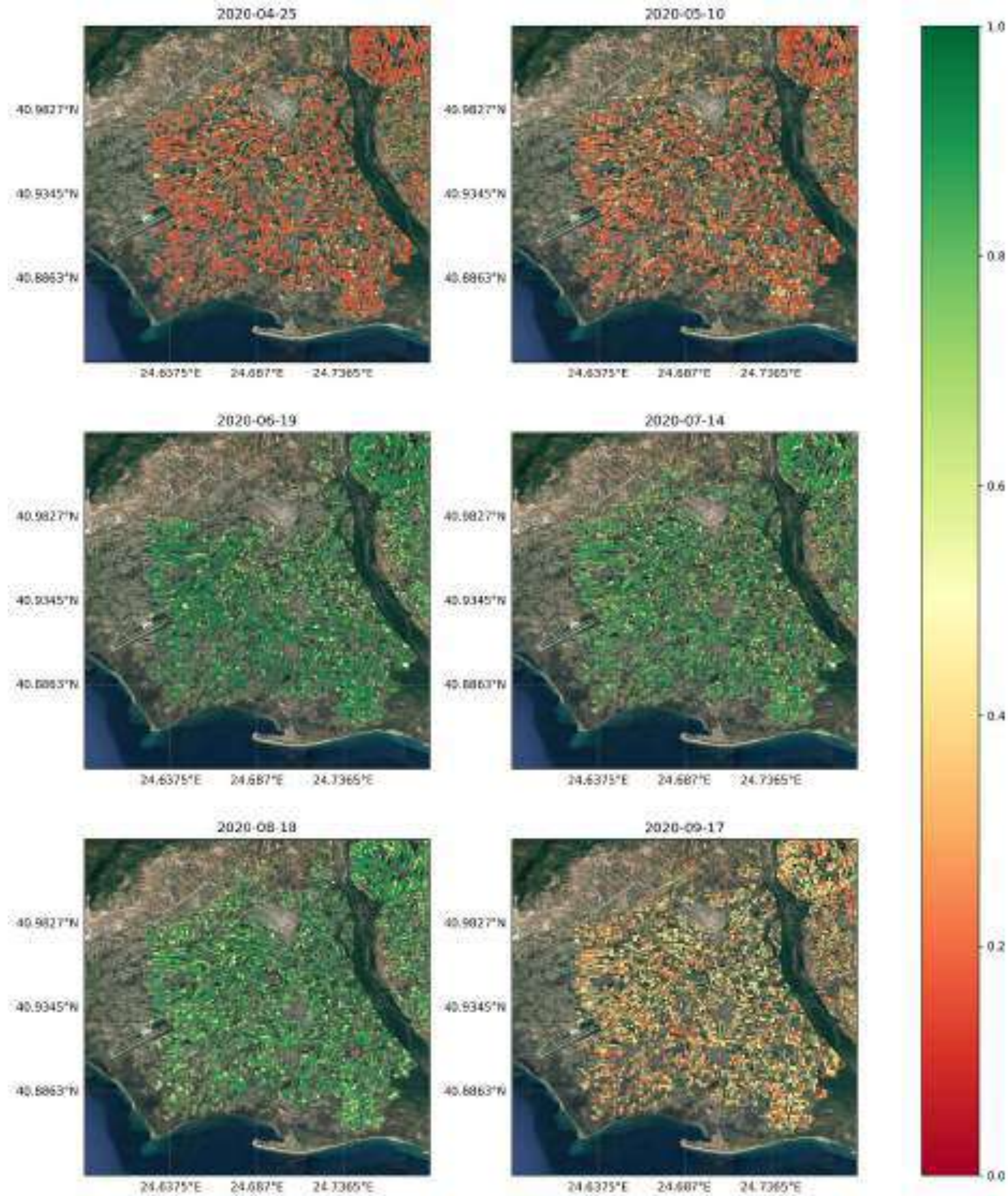

Figure 18. NDVI development through 2020 cultivation season for maize crop.

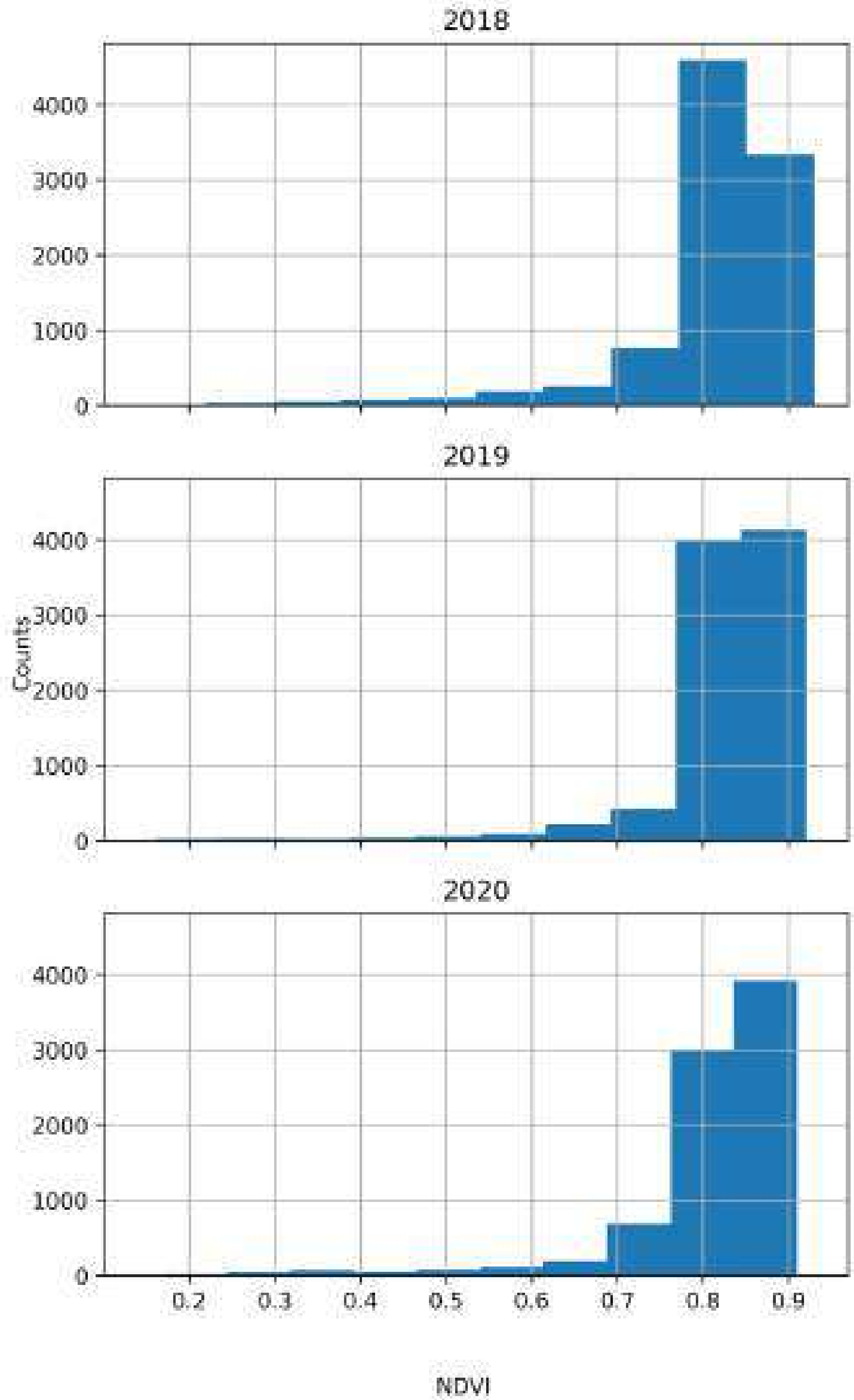

Figure 19. Histograms of maize crop NDVI on 15/7/2018, 25/7/2019 and 14/7/2020.

3.2.2 Maize NDVI characteristic curves

In order to obtain the pattern of the NDVI development for maize crop within the study area, a polynomial model was fitted to the mean NDVI values (the average NDVI of all the fields for a given date) obtained from all the available NDVI maps that were derived from Sentinel 2 products for each of the three years (Table 36, Figure 20). To do that the following polynomial function was used:

$$NDVI = ax^3 + bx^2 + cx + \text{intercept} \quad (18)$$

where x was the day of year.

The analysis showed that the model described the maize NDVI development with adequate precision when the data of each year were processed separately. Multiple R^2 and adjusted R^2 were found to be equal to or higher than 0.95 (Table 36), whilst residual error fluctuated between -0.1 and 0.1 (Figure 20).

Similarly good results were obtained when the data of all years were aggregated and processed together. Again, multiple R^2 and adjusted R^2 reached satisfactory values (0.95 both), while residual error range stayed almost the same taking values from -0.12 to 0.1.

It is noteworthy that the estimated errors for the polynomial model coefficients were considerably y low for all cases, showing values that ranged from ±0.01 to ±0.05 (Table 37).

Table 36. Regression analysis results on NDVI values during the maize growing cycle in 2018, 2019 and 2020. *Fitting model f(x) = ax^3+bx^2+x+intercept*

Year	a	b	c	intercept	Multiple R^2	Adj. R^2
2018	0.35±0.03	-0.54±0.03	-0.09±0.03	0.57±0.01	0.99	0.98
2019	0.77±0.05	-0.49±0.05	-0.34±0.05	0.51±0.01	0.96	0.95
2020	0.56±0.05	-0.46±0.05	-0.15±0.05	0.66±0.01	0.95	0.94
Agg.	1.05±0.05	-0.90±0.05	-0.41±0.05	0.57±0.01	0.95	0.95

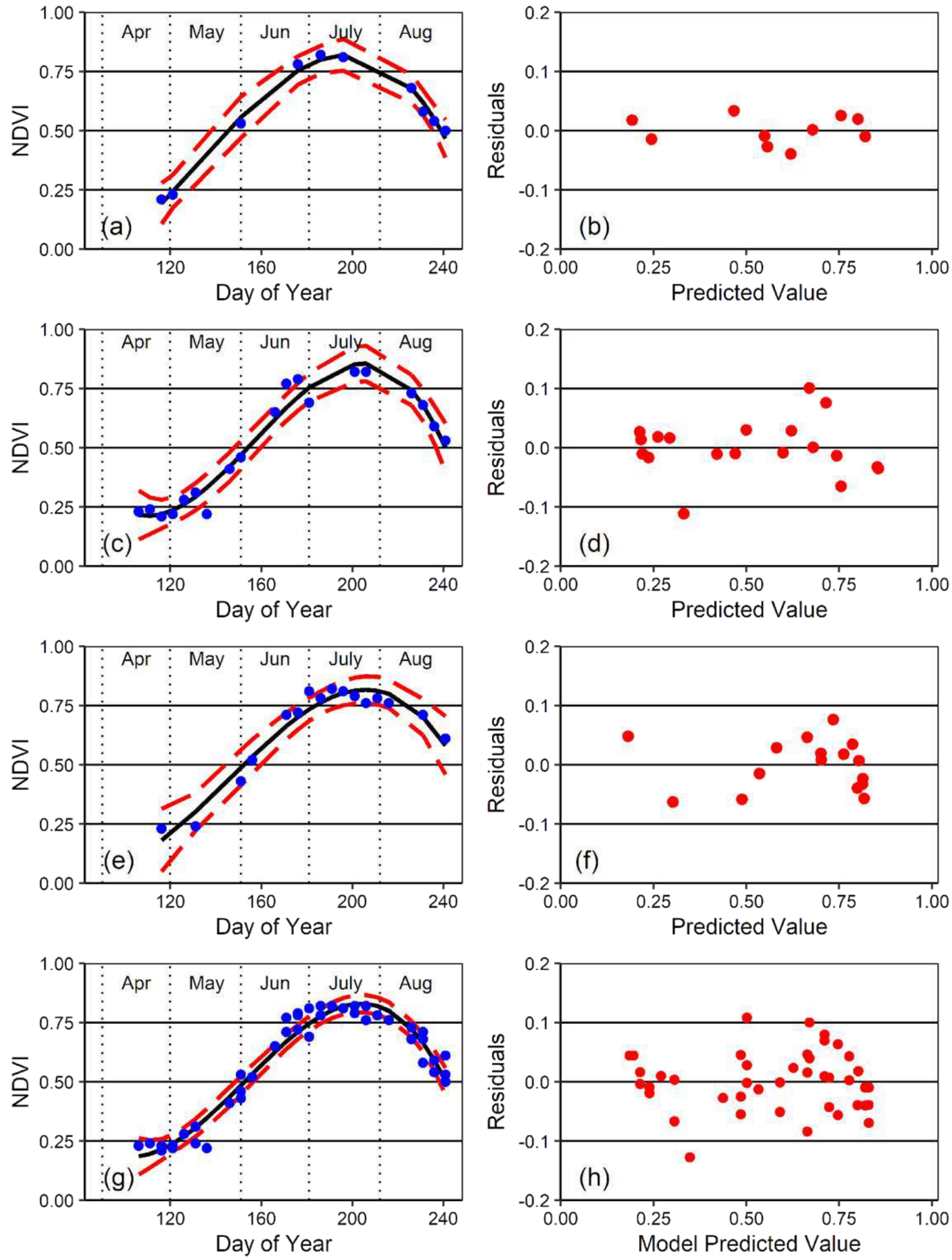

Figure 20. Mean NDVI values and fitting curves for (a) 2018; (c) 2019; (e) 2020; (g) all the years. Residuals between the observed and simulated NDVI values for (b) 2018; (d) 2019; (f) 2020; (h) all the years.

3.2.3 Rice NDVI data

The development of NDVI index throughout the 2018, 2019 and 2020 cultivation seasons for rice crop are illustrated in Figures 21, 22 and 23, respectively. The rice seeds were usually sowed in the first week of May within the study area, and they germinate within 5 - 10 days from sowing. The sowing density was so dense that even right after emergence, the young rice plants cover a moderate part of the field. As a result, even since late May the rice fields NDVI values were above 0.6 (Figure 21, 22).

For all years the NDVI values were found to be considerably high (> 0.8) during June, July, August, and early September and then started to gradually decline as the crop reaches maturity.

Despite the general trend that was observed in the majority of the fields for all years, there were cases in which the fields received NDVI values that did not follow the general trend. For instance, there were fields in which their NDVI values were lower than the mean during the whole cultivation season or in some specific development stage. It is difficult to report whether these low values were attributed to poor irrigation and fertilization, pests' infection, canopy damage from hail storms or some other reason, but it is rather clear that plants in these fields experience stress, and thus their final yield will not be optimum.

One of the key growing stages that low NDVI values could lead to a potential decrease in rice yield is July, during which rice seed formation is happening. Figure 24 shows the number of fields experiencing stress, i.e., have NDVI values lower than 0.8 on July 15, July 25 and July 14 in 2018, 2019 and 2020, respectively. Specifically, on July 15, 2018, approximately 87 fields out of 924 (roughly 9.4%) were found to exhibit NDVI values lower than 0.8. The number of stressed fields was considerably lower in 2019, equal to 39 out of 664 (approximately 5.9%), but increased again substantially in 2020 to reach 141 stressed fields out of 715 (around 19.7%).

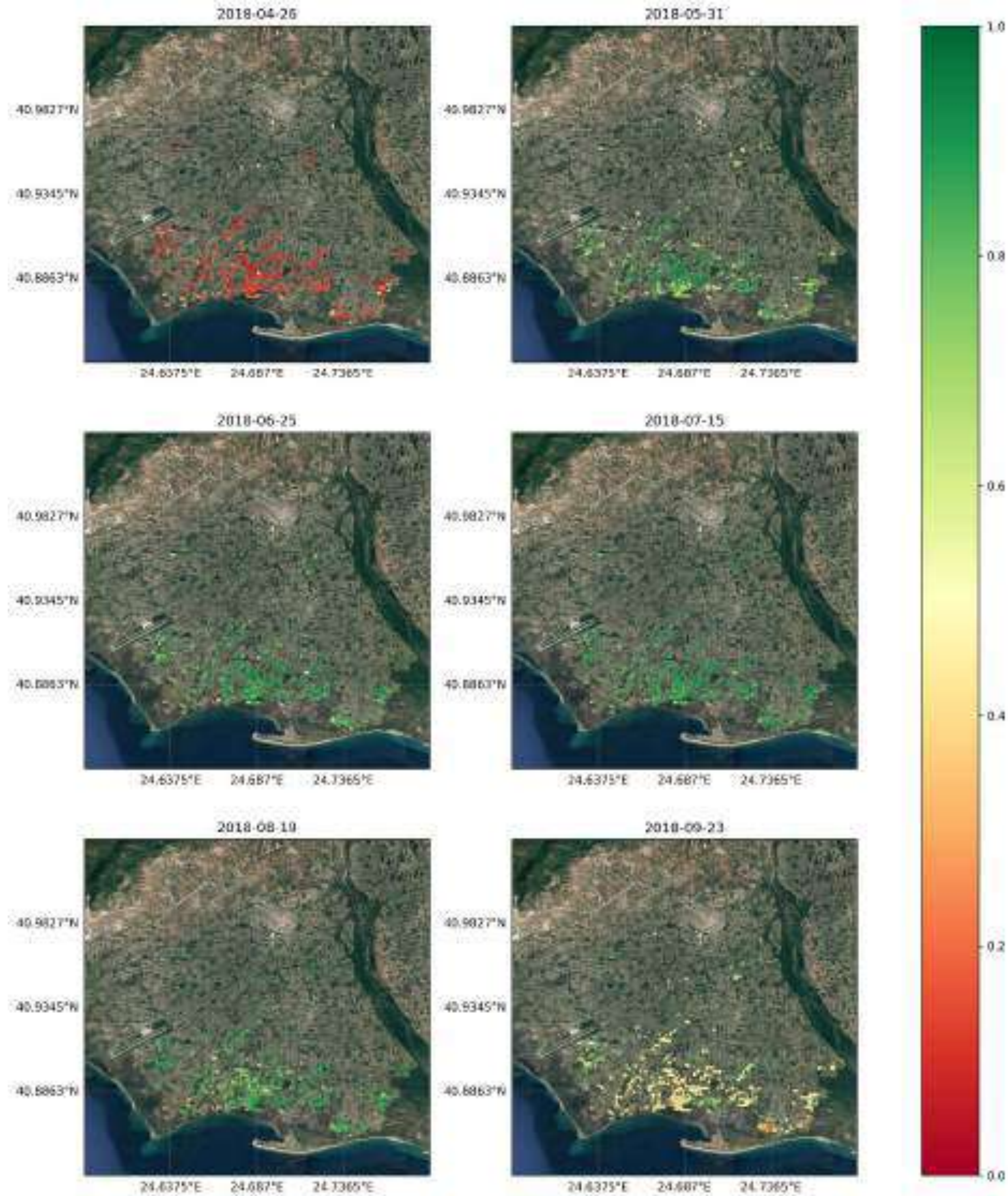

Figure 21. NDVI development through 2018 cultivation season for rice crop.

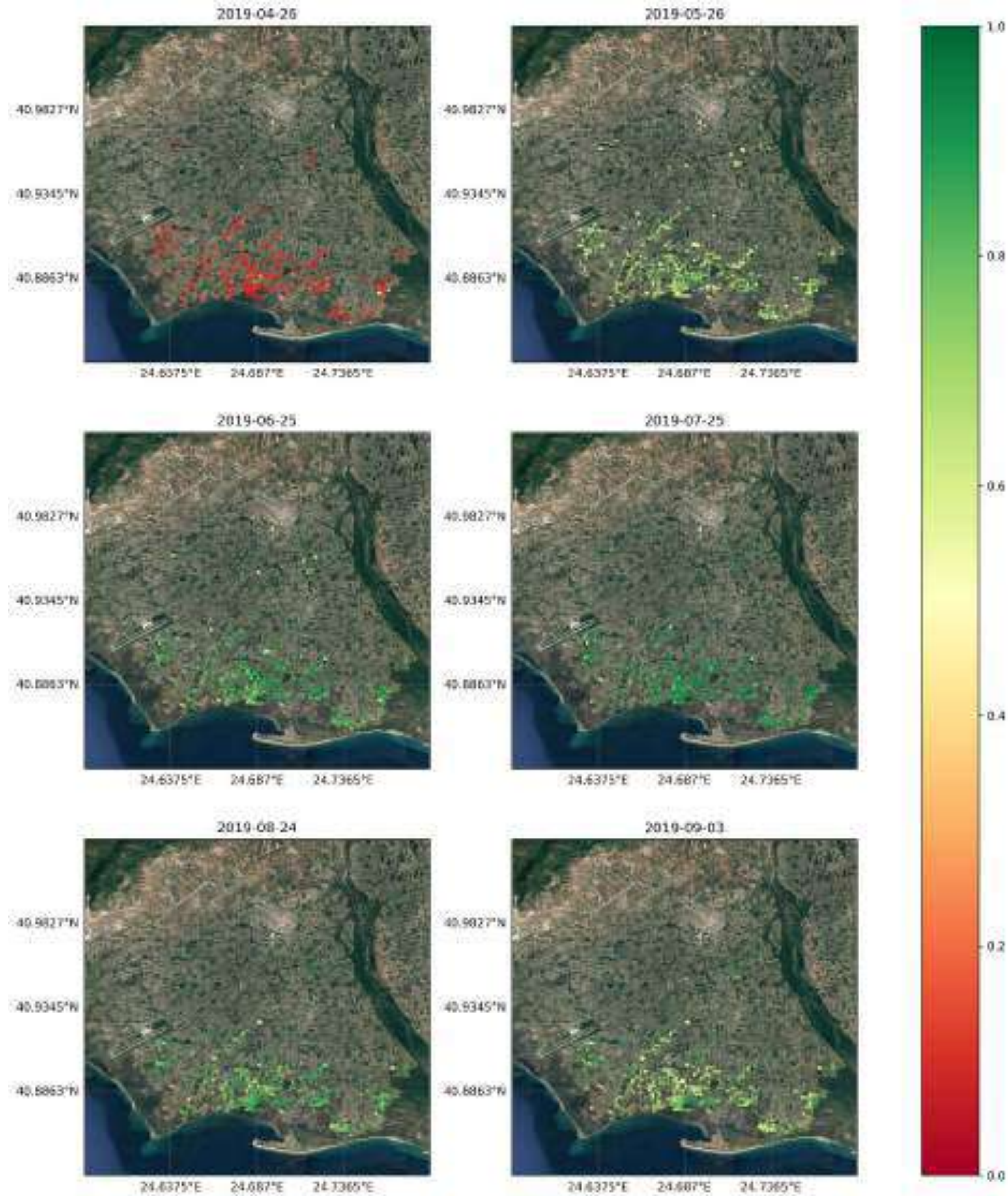

Figure 22. NDVI development through 2019 cultivation season for rice crop.

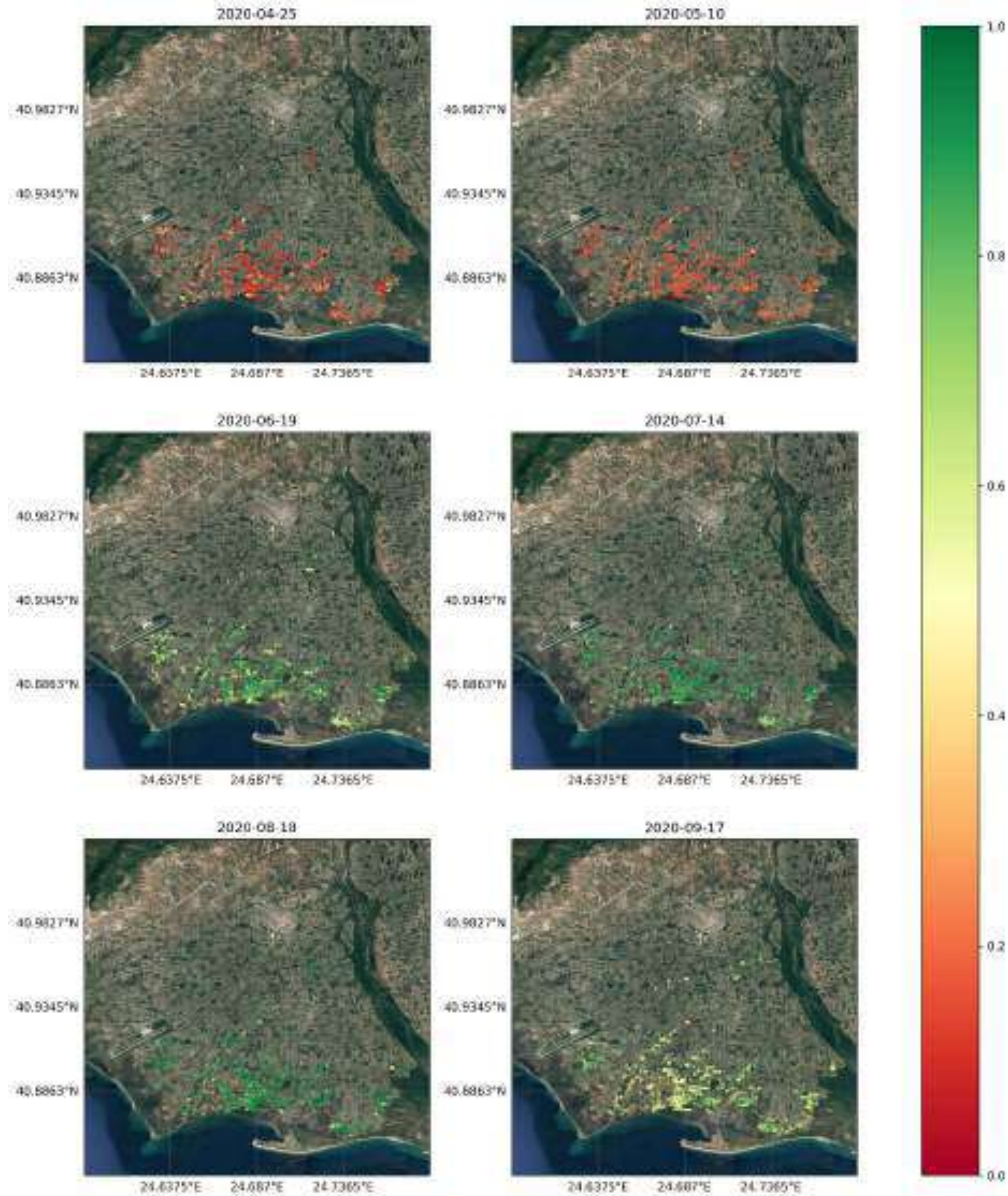

Figure 23. NDVI development through 2020 cultivation season for rice crop.

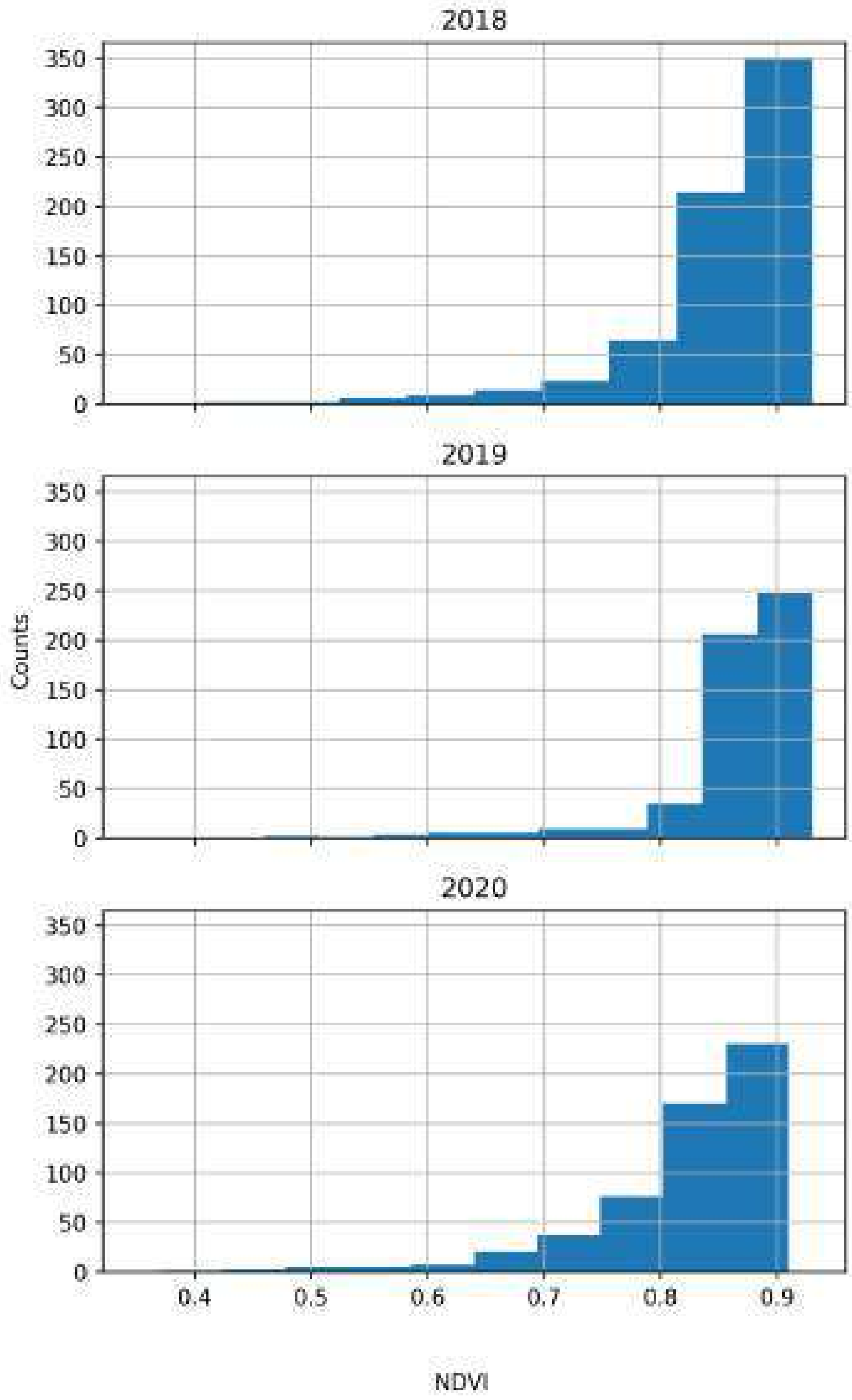

Figure 24. Histograms of rice crop NDVI on 15/7/2018, 25/7/2019 and 14/7/2020.

3.2.4 Rice NDVI characteristic curves

In order to obtain the pattern of the NDVI development for rice crop within the study area, the Eq. (1) implemented in sub-section 3.2.2 "*Maize NDVI characteristic curves*" was used. Data obtained from all the available NDVI maps that were derived from Sentinel 2 products for each of the three years were used for the analysis.

The analysis showed that the model can potentially predict the rice NDVI development with adequate precision, when the data of each year were processed separately. Multiple R^2 and adjusted R^2 were found to be equal to or higher than 0.95 (Table 37). For 2018 residual error was found to be very similar to that of maize taking values that ranged between -0.1 and 0.1, whilst for 2019 and 2020 residual error was considerably higher fluctuating between -0.2 and 0.1 (Figure 25).

As in the case of maize, fairly good results were obtained when the data of all years were aggregated and processed together, as well. Again, Multiple R^2 and adjusted R^2 obtained satisfactory values (0.95 both), while the residual error range remained almost the same with values from -0.2 to 0.11.

The estimated errors for the polynomial model coefficients were found to be remarkably low for the rice crop and for all the cases, showing values that ranged from ±0.01 to ±0.04 (Table 22).

Table 37. Regression analysis results on NDVI values during cotton growing cycle in 2018, 2019 and 2020. Fitting model $f(x) = ax^3+bx^2+x+intercept$

Year	a	b	c	intercept	Multiple R^2	Adj. R^2
2018	0.62±0.02	0.06±0.02	-0.16±0.02	0.51±0.01	0.99	0.99
2019	0.85±0.04	0.20±0.04	-0.20±0.04	0.41±0.01	0.97	0.97
2020	0.55±0.02	0.08±0.02	-0.11±0.02	0.45±0.00	0.99	0.99
Agg.	1.20±0.04	0.24±0.04	-0.25±0.04	0.45±0.01	0.96	0.96

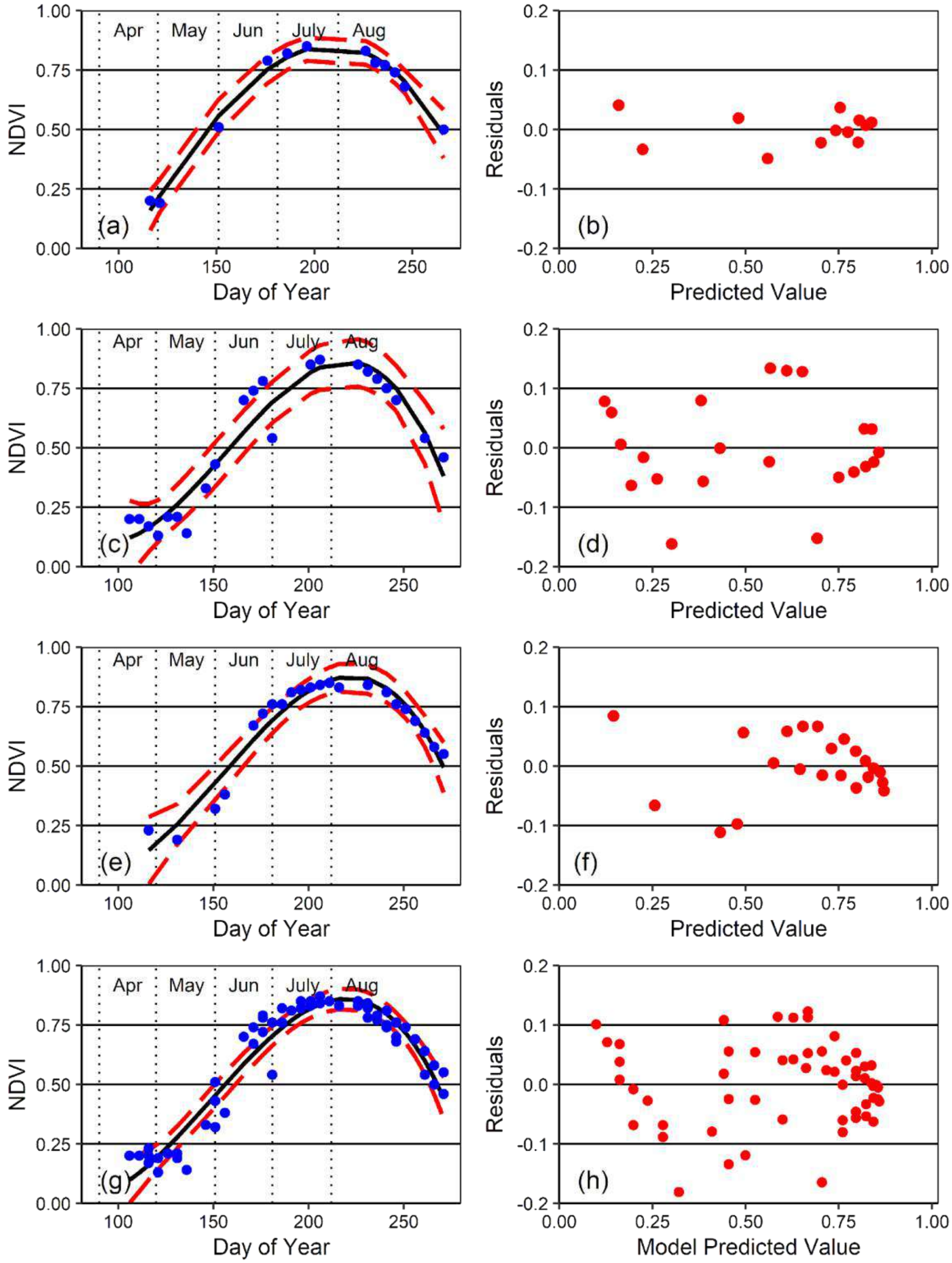

Figure 25. Mean NDVI values and fitting curves for rice crop for (a) 2018; (c) 2019; (e) 2020; (g) all the years. Residuals between the observed and simulated NDVI values for (b) 2018; (d) 2019; (f) 2020; (h) all the years.

3.2.5 Cotton NDVI data

Cotton seeds were planted in the study area during the first ten days of May and ideally germinate in about 10-15 days. The development of the NDVI index throughout the 2018, 2019 and 2020 cultivation seasons for cotton are illustrated in Figures 26, 27 and 28, respectively. As a result, in 2018 and 2019 the NDVI values during April and May were found to be around 0.3 or lower. However, in April 2020 the NDVI values showed values close to 0.5. This can be attributed to the existence of weeds within the fields or to an error during the Sentinel 2 image processing and conversion to NDVI via the sen2r tool (sub-section 2.2 "*Copernicus Sentinel 2 mission imagery*").

During June and July, the cotton plants' canopy developed rapidly, reaching its maximum value of 0.75 in 2018 and 2019. The mean maximum value was found to be moderately lower in 2020, being equal to 0.7. This lower maximum indicates that due to the 2020 weather conditions, the cotton plants failed to reach their optimum development.

As in the case of maize and rice, all the cotton fields did not follow the general trend that was observed in most fields for all years. By closely observing Figures 26 to 28 it is obvious that there were fields in which the NDVI did not exceed 0.5 even in August.

In a similar manner to maize and rice cases, the cause of these low NDVI values seems difficult to be diagnosed as it may be attributed to excessive irrigation, poor fertilization, pests' infection, canopy damage from hail storms or some other reason. However, it is certain that plants in these fields experienced stress, and thus their final yield was not optimum.

The cotton NDVI-values in August serve as a good indicator to assess a potential decrease in the final crop yield. Figure 29 shows the number of fields that experienced stress, exhibiting NDVI values lower than 0.65 on August 19, August 24 and August 18 in 2018, 2019 and 2020, respectively. In detail, on August 19, 2018, 292 fields out of 1,567 (roughly 18.6%) were found to exhibit NDVI values lower than 0.8. The number of stressed fields was considerably lower in 2019, being equal to 419 out of 1,994 (18.3%), but increased again significantly in 2020 to reach 543 stressed fields out of 715 (27.2%). It worth mentioning that the cotton fields which experience stress conditions when compared to maize and rice fields are at least three times higher for all years.

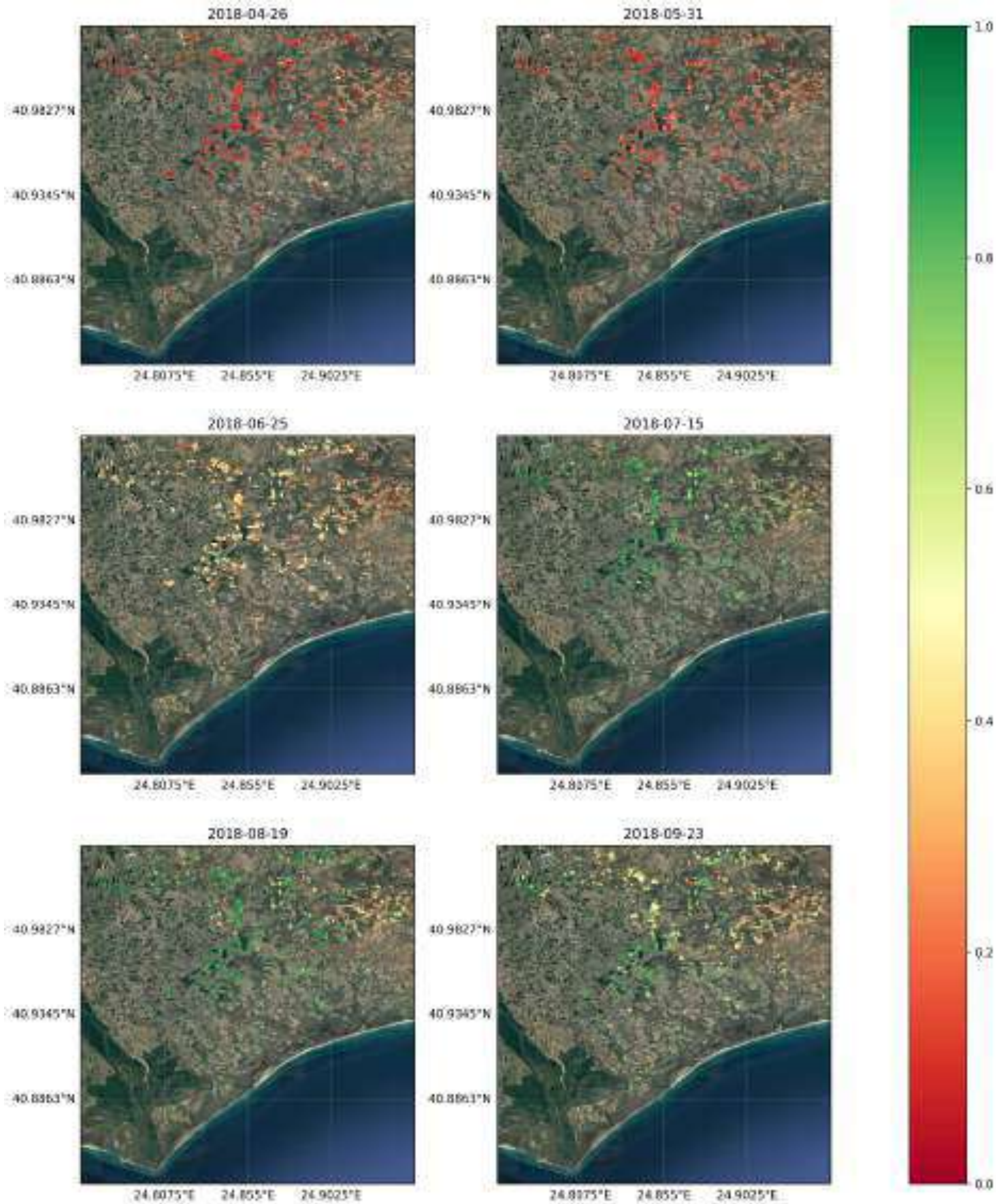

Figure 26. NDVI development through 2018 cultivation season for cotton crop.

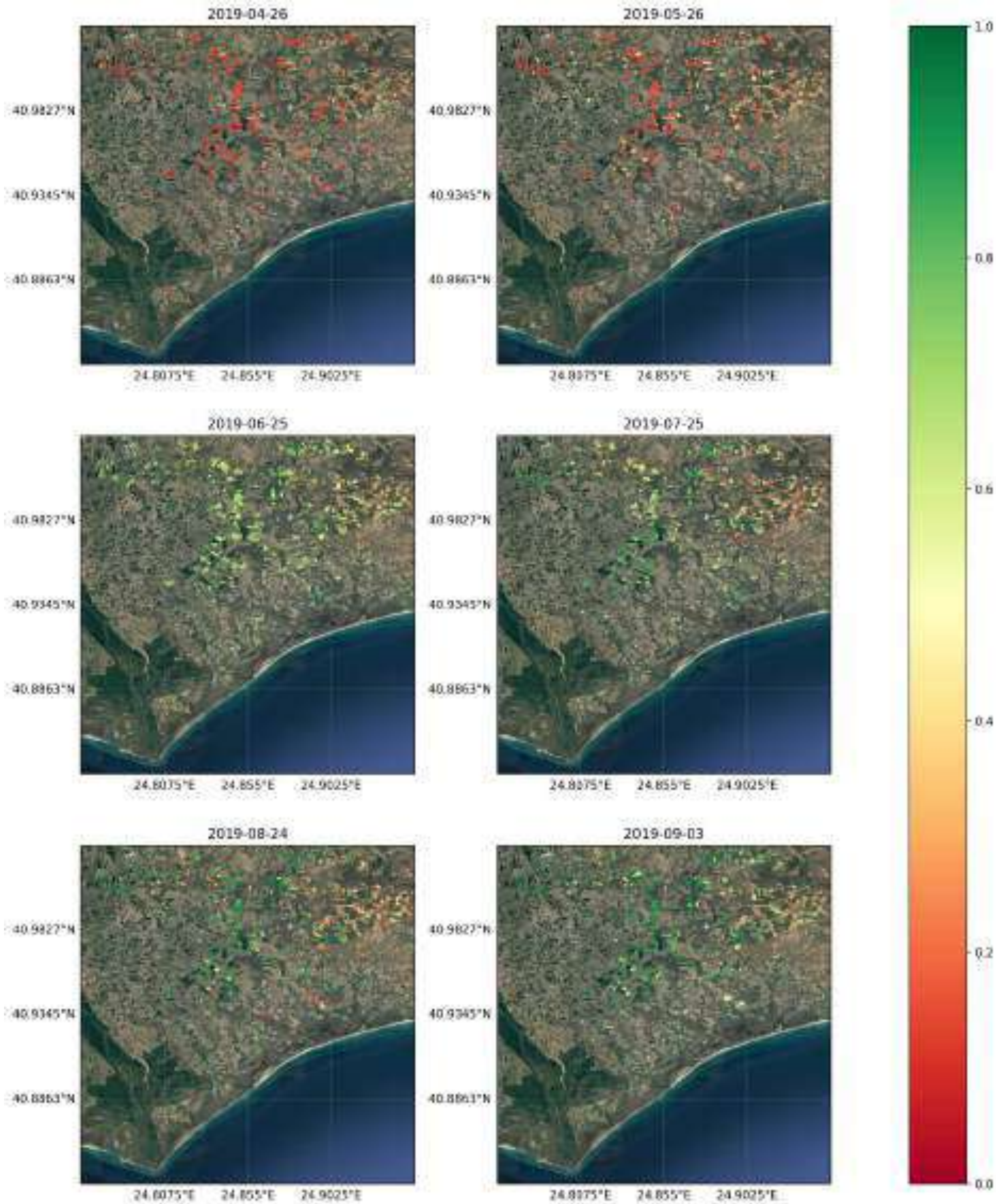

Figure 27. NDVI development through 2019 cultivation season for cotton crop.

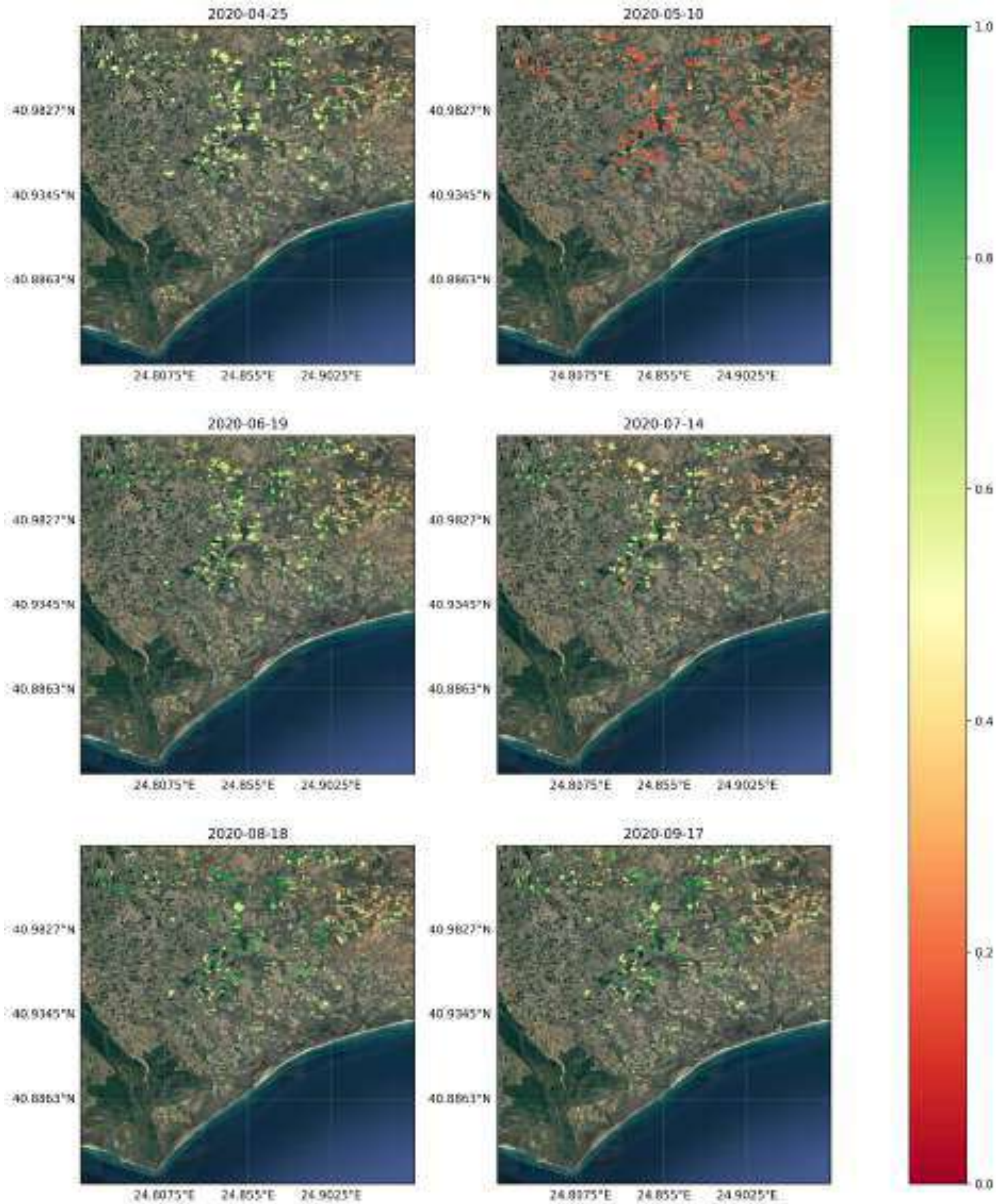

Figure 28. NDVI development through 2020 cultivation season for cotton crop.

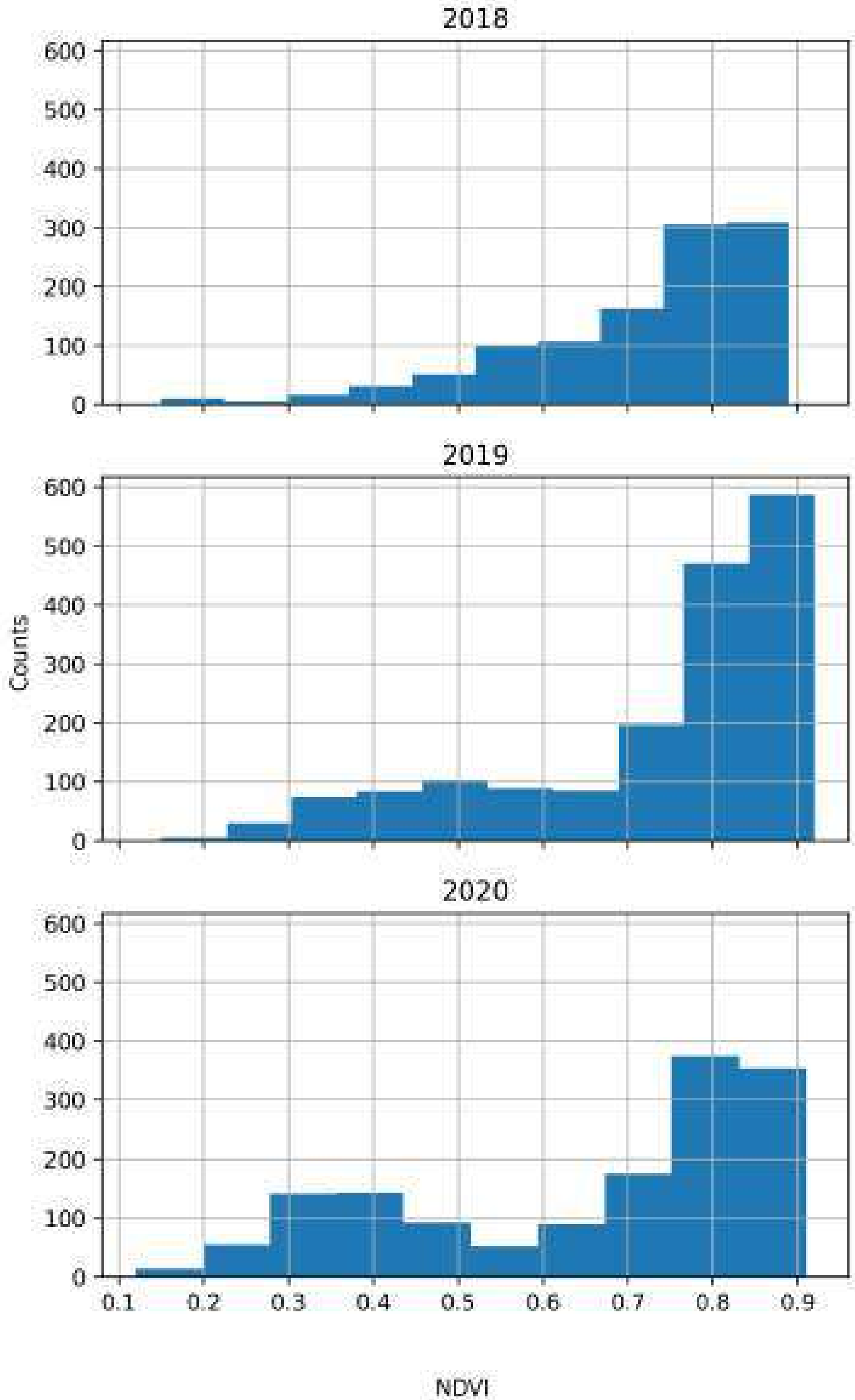

Figure 29. Histograms of cotton crop NDVI on 18/9/2018, 24/8/2019 and 18/8/2020.

3.2.6 Cotton NDVI characteristic curves

The cotton NDVI development curve was obtained using the Eq. (1) implemented in sub-section 3.2.2 "*Maize NDVI characteristic curves*" was used. Data obtained from all the available NDVI maps that were derived from Sentinel 2 products for each of the three years were used for the analysis.

The analysis showed that the model described the cotton NDVI development with adequate precision when the data of each year were processed separately. Multiple R^2 and adjusted R^2 were found to be equal to or higher than 0.96 (Table 38), whilst residual error fluctuated between -0.1 and 0.1 (Figure 30).

Similarly good results were obtained when the data of all years were aggregated and processed together. Again, Multiple R^2 and adjusted R^2 reached satisfactory values (0.96 both), while residual error range stayed almost the same taking values from -0.08 to 0.1.

It is noteworthy that the estimated errors for the polynomial model coefficients were considerably low for all cases, showing values that ranged from ±0.01 to ±0.04 (Table 38).

Table 38. Regression analysis results on NDVI values during cotton growing cycle in 2018, 2019 and 2020. Fitting model $f(x) = ax^3+bx^2+x+intercept$

Year	a	b	c	intercept	Multiple R^2	Adj. R^2
2018	0.62±0.02	0.06±0.02	-0.16±0.02	0.51±0.01	0.99	0.99
2019	0.85±0.04	0.20±0.04	-0.20±0.04	0.41±0.01	0.97	0.97
2020	0.55±0.02	0.08±0.02	-0.11±0.02	0.45±0.00	0.99	0.99
Agg.	1.20±0.04	0.24±0.04	-0.25±0.04	0.45±0.01	0.96	0.96

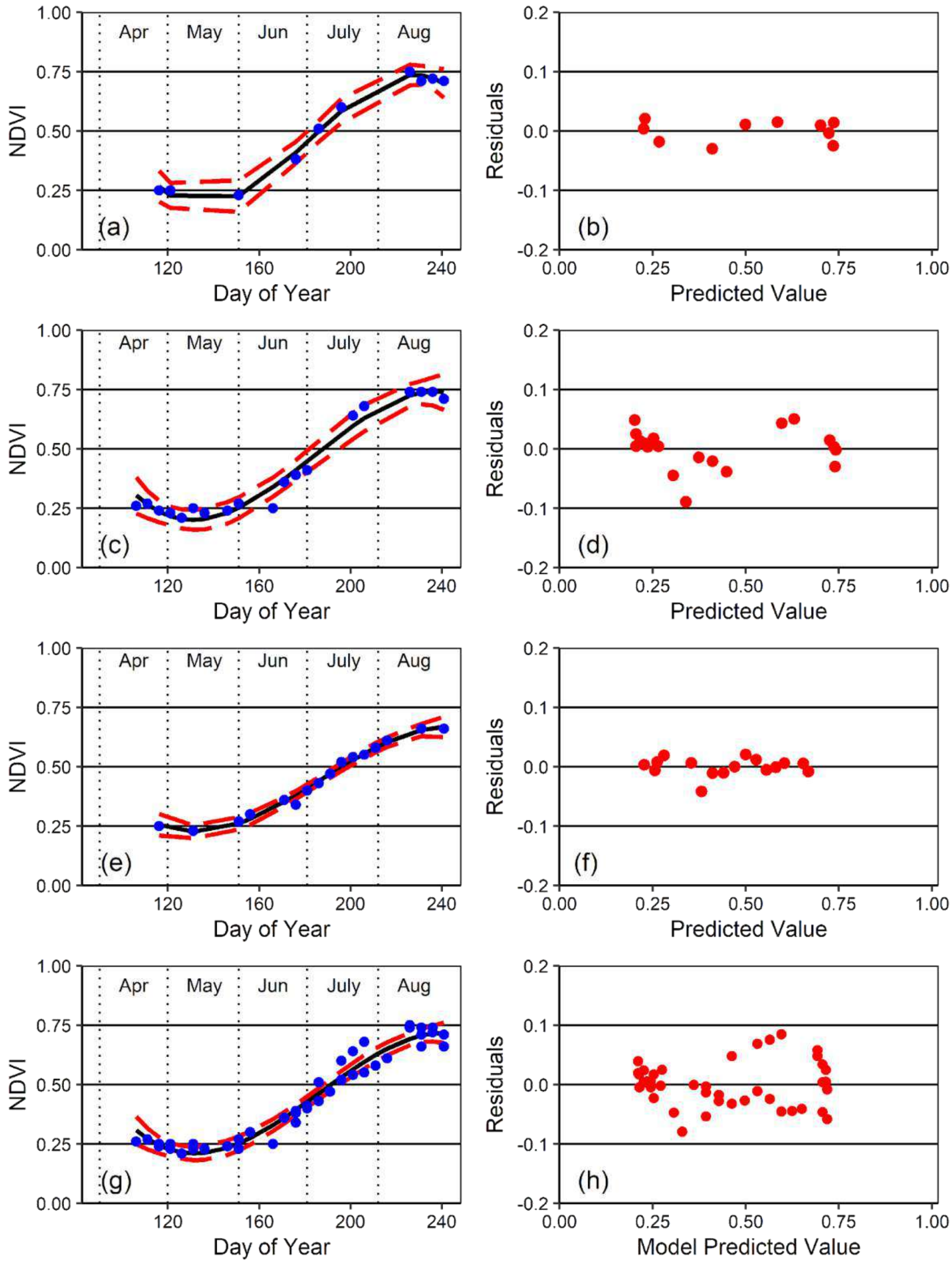

Figure 30. NDVI mean values and fitting curves for cotton crop for (a) 2018; (c) 2019; (e) 2020; (g) all the years. Residuals between the observed and simulated NDVI values for (b) 2018; (d) 2019; (f) 2020; (h) all the years.

3.2.7 Maize WF

To access the impact of soil hydraulic properties variations (as those analyzed in detail in the sub-section 3.1 "*Variations of soil hydraulic properties*") on WF values, three soil files created and used in AquaCrop model. For the creation of the first file, named 'low", we used the lowest FC and PWP values within each class. Accordingly, the second file, named "mean", integrated the mean FC and PWP values, while the third one, "max", the corresponding maximum values. The textural classes that were used for the case of maize were loam, sandy loam and sandy clay loam, as in the clay loam fields farmers tend to cultivate cotton as the crop maps revealed.

Still in 2018, the results showed that, when the farmer empirical irrigation scheduling was used, the WF values ranged between 279.2 to 318.5 m^3/t (Table 39, Figure 31). It is worth mentioning that in average, the lowest WF values were observed in the case of sandy loam textural class (259-290 m^3/t). On the other hand, loams exhibited the highest WF values. For all the textural classes the green WF component represented roughly 34-41% of the total, whilst blue WF ~58-65%.

When the WF obtained by the implementation of the empirical irrigated fields was compared to the one derived from the implementation of the optimum irrigation scenario, it is revealed that farmer irrigation performance can be considerably improved. In detail, WF under the optimum irrigation scenario did not exceed the 260 m^3/t for all the textural classes (Table 39). Moreover, the contribution of green WF component found to be slightly higher than the empirical case ranging from 39% to 41%. It should be noted that, the optimal total WF was 43%, 53%, 64%, 4%, 26%, 23%, 19%, 32% and 27% for loam low, loam mean, loam max, sandy loam low, sandy loam mean, sandy loam max, sandy clay loam low, sandy clay loam mean and sandy clay loam max scenarios, respectively.

Table 39. Descriptive WF data for empirical and optimal irrigated maize fields in 2018.

	Empirical			Optimal		
	WF_green	**WF_blue**	**WF**	**WF_green**	**WF_blue**	**WF**
Lo low	101.6	195.6	297.2	104.3	150.0	254.3
Lo mean	116.0	192.0	308.0	112.6	142.2	254.8
Lo max	131.8	186.7	318.5	112.6	142.2	254.8
SaLo low	76.7	183.2	259.9	82.4	173.2	255.6
SaLo lean	99.4	183.0	282.4	101.7	154.4	256.1
SaLo lax	111.9	179.1	291.0	115.2	153.1	268.3
SaClLo low	101.6	177.6	279.2	106.2	154.5	260.7
SaClLo mean	113.2	176.8	290.0	112.0	146.1	258.0
SaClLo max	122.2	170.2	292.4	121.6	144.1	265.7

Lo=loam; SaLo=sandy loam; SaClLo = sandy clay loam

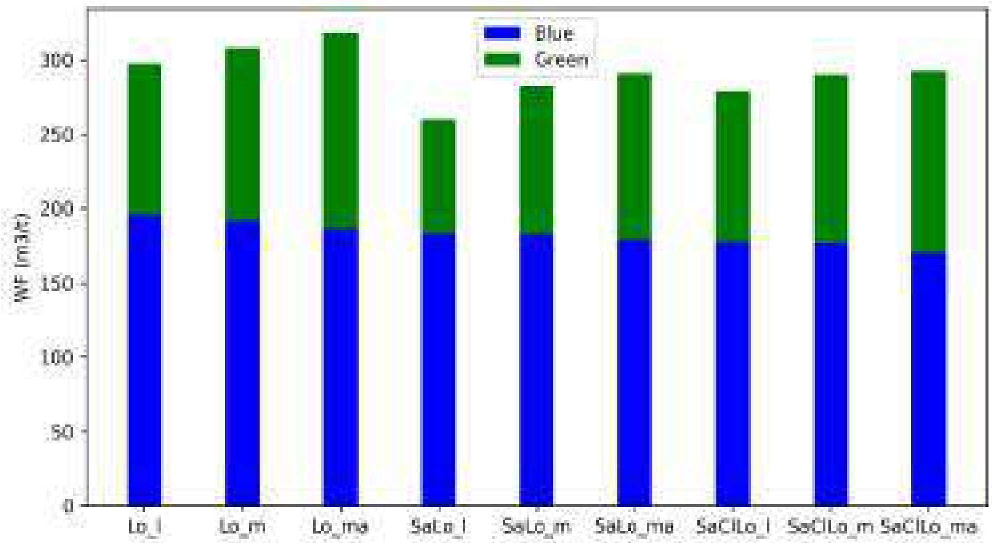

Figure 31. Green and Blue maize WF when implemented a farmer empirical irrigation in 2018 for loam, sandy loam, and sandy clay loam soils. *Lo_l=Loam low end variations; Lo_m=Loam mean variation; L_ma=Loam up end variatons; SaLo_l=Sandy Loam low end variations; SaLo_m=Sandy Loam mean variation; SaLo_ma=Sandy Loam up end variations; SaClLo_l=Sandy Clay Loam low end variations; SaClLo_m=Sandy Clay Loam mean variation; SaClLo_ma=Sandy Clay Loam up end variations.*

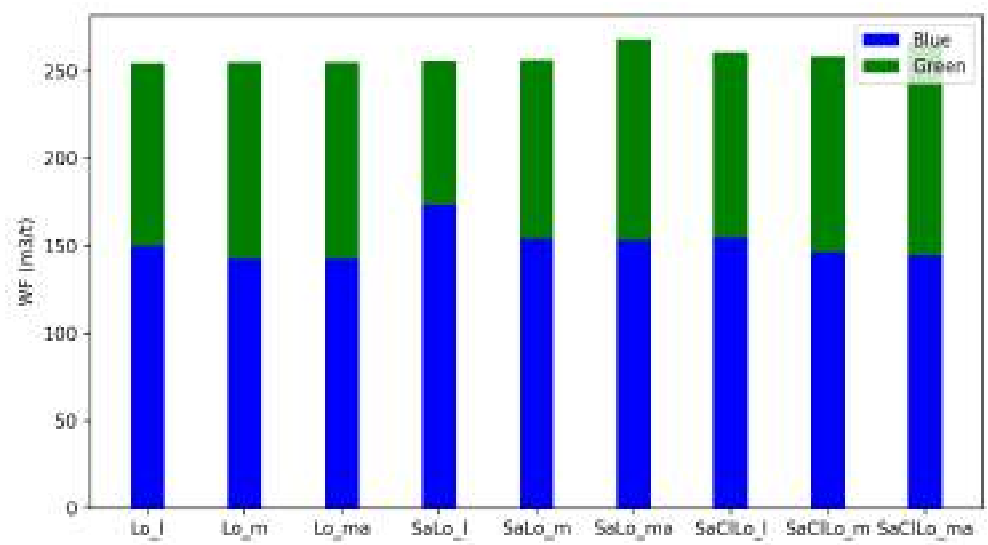

Figure 32. Green and Blue maize when implemented an optimized irrigation in 2018 for loam, sandy loam, and sandy clay loam soils. *Lo_l=Loam low end variations; Lo_m=Loam mean variation; L_ma=Loam up end variatons; SaLo_l=Sandy Loam low end variations; SaLo_m=Sandy Loam mean variation; SaLo_ma=Sandy Loam up end variations; SaClLo_l=Sandy Clay Loam low end variations; SaClLo_m=Sandy Clay Loam mean variation; SaClLo_ma=Sandy Clay Loam up end variations.*

In 2109, the total WF found to be lower that of 2018, taking its' maximum value of 278 m^3/t in the case of loam max scenario (Table 40). Again, the lower WF values, in average, were observed for sandy loam fields (Figure 33). This year, the green WF component contribution was slightly lower than 2018, fluctuating from 28% to 39%, and thus the blue WF component showed contribution values up to 72%.

In the case of the implementation of optimal irrigation scenario in 2019, the maximum total WF was observed of the loam max scenario similarly to the empirical irrigation (Table 40), but it was approximately 8% lower (262 m^3/t) than the corresponding empirical one. In general, the total WF values derived under the optimum irrigation scenario were found to be 7-10% lower than the corresponding empirical ones. It is noteworthy, that excluding all lower values, the optimum irrigation scenario showed less deviation among the different textural classes and a more consistent performance overall (Figure 34).

Table 40. Descriptive WF data for empirical and optimal irrigated maize fields in 2019.

	Empirical			Optimal		
	WF_green	**WF_blue**	**WF**	**WF_green**	**WF_blue**	**WF**
Lo low	89.7	180.0	269.7	111.6	145.3	256.8
Lo Mean	99.8	176.9	276.7	117.5	137.4	254.9
Lo Max	110.3	167.8	278.0	130.1	132.1	262.2
SaLo low	69.7	174.0	243.8	91.8	160.4	252.2
SaLo Mean	91.1	178.9	270.0	114.2	142.6	256.9
SaLo Max	101.6	172.4	274.0	121.5	138.0	259.5
SaClLo low	93.7	175.4	269.0	113.6	144.6	258.2
SaClLo mean	103.8	172.9	276.7	122.2	136.7	258.9
SaClLo Max	108.9	167.1	276.0	124.8	131.4	256.2

Lo=loam; SaLo=sandy loam; SaClLo = sandy clay loam

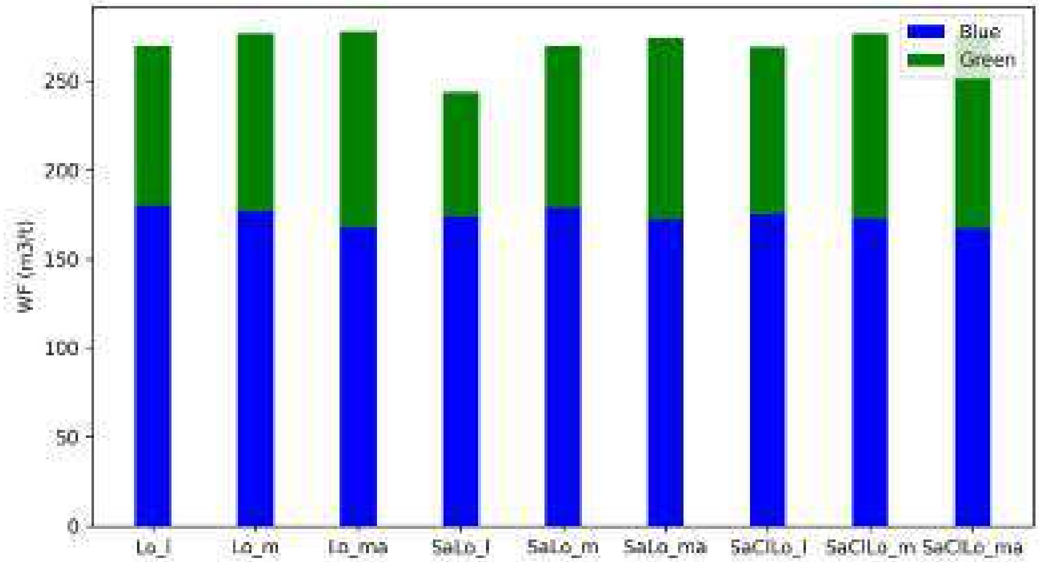

Figure 33. Green and Blue maize WF when implemented a farmer empirical irrigation in 2019 for loam, sandy loam, and sandy clay loam soils. *Lo_l=Loam low end variations; Lo_m=Loam mean variation; L_ma=Loam up end variatons; SaLo_l=Sandy Loam low end variations; SaLo_m=Sandy Loam mean variation; SaLo_ma=Sandy Loam up end variations; SaClLo_l=Sandy Clay Loam low end variations; SaClLo_m=Sandy Clay Loam mean variation; SaClLo_ma=Sandy Clay Loam up end variations.*

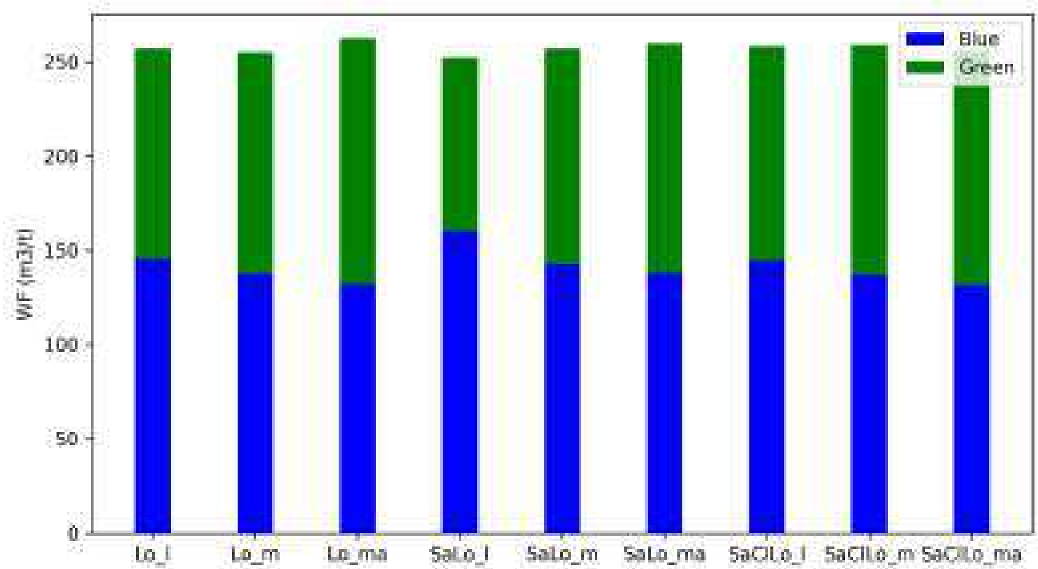

Figure 34. Green and Blue maize WF when implemented an optimized irrigation in 2019 for loam, sandy loam, and sandy clay loam soils. *Lo_l=Loam low end variations; Lo_m=Loam mean variation; L_ma=Loam up end variatons; SaLo_l=Sandy Loam low end variations; SaLo_m=Sandy Loam mean variation; SaLo_ma=Sandy Loam up end variations; SaClLo_l=Sandy Clay Loam low end variations; SaClLo_m=Sandy Clay Loam mean variation; SaClLo_ma=Sandy Clay Loam up end variations.*

The implementation of the empirical irrigation scenario in 2020 resulted in significant variations among the various scenarios (Figure 35), but also scored the largest total WF (330 m^3/t) among all the years. Within the loam textural class, total WF showed values that ranged from 199 m^3/t to 284 m^3/t, a difference almost equal to 90 m^3/t (Table 41). Even more strikingly, in the case of sandy clay loam total WF plummeted from 330 m^3/t for max scenario to 200 m^3/t for low scenario. The contribution of the green WF component was found to be almost identical to this of 2019, fluctuating between 26% and 41%.

When the optimal irrigation was implemented, the variations within classes were minimized resulted in an average total WF equal to 270 m^3/t (Figure 36). It should be mentioned that while in all the implemented scenarios the total WF under optimal irrigation was found to be lower than that of the empirical (8-26%), while in the case of the sandy clay loam low scenario the empirical irrigation was found to perform better by roughly 30%. The overall contribution of the green WF component was found to be substantially higher when compared to the empirical one showing values 37%-53%

Table 41. Descriptive WF data for empirical and optimal irrigated maize fields in 2020.

	Empirical			Optimal		
	WF_green	**WF_blue**	**WF**	**WF_green**	**WF_blue**	**WF**
Lo low	95.40	189.48	284.88	123.9	144.9	268.7
Lo Mean	111.18	186.86	298.04	133.7	138.3	272.0
Lo Max	142.38	199.18	341.56	152.7	132.4	285.1
SaLo low	68.24	189.48	257.72	99.0	165.2	264.1
SaLo Mean	98.45	191.55	290.00	116.0	149.4	265.5
SaLo Max	125.72	205.24	330.96	129.8	137.6	267.4
SaClLo low	76.19	127.87	204.05	121.3	150.1	271.4
SaClLo mean	111.85	184.18	296.03	134.4	140.3	274.6
SaClLo Max	132.54	199.18	331.72	140.3	137.6	277.9

Lo=loam; SaLo=sandy loam; SaClLo = sandy clay loam

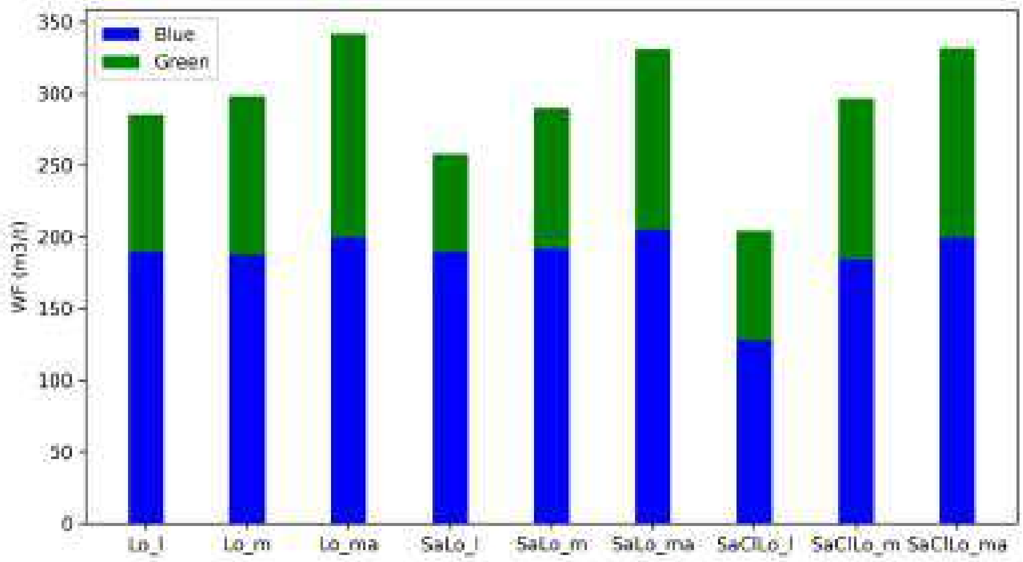

Figure 35. Green and Blue maize WF when implemented a farmer empirical irrigation in 2020 for loam, sandy loam, and sandy clay loam soils. *Lo_l=Loam low end variations; Lo_m=Loam mean variation; L_ma=Loam up end variatons; SaLo_l=Sandy Loam low end variations; SaLo_m=Sandy Loam mean variation; SaLo_ma=Sandy Loam up end variations; SaClLo_l=Sandy Clay Loam low end variations; SaClLo_m=Sandy Clay Loam mean variation; SaClLo_ma=Sandy Clay Loam up end variations.*

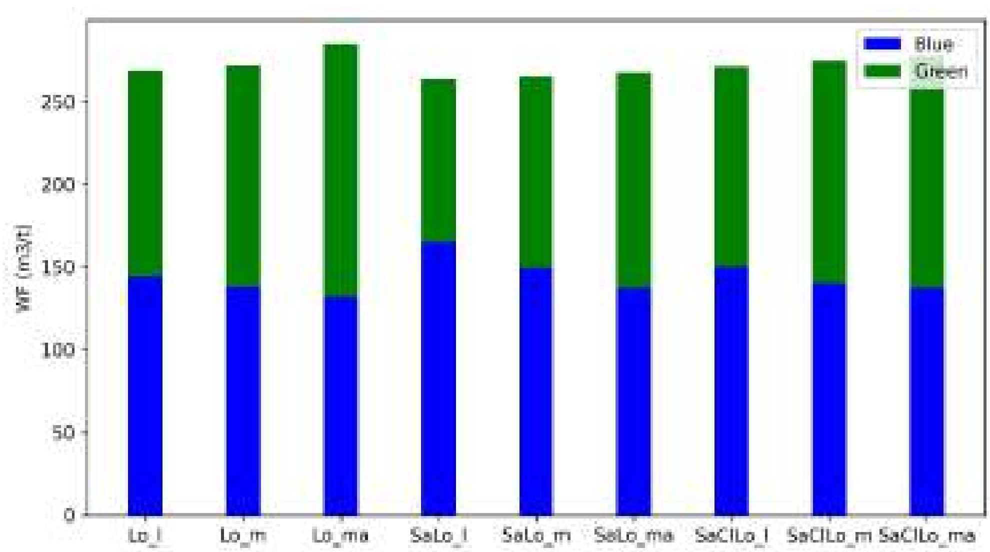

Figure 36. Green and Blue maize WF when implemented an optimized irrigation in 2020 for loam, sandy loam, and sandy clay loam soils. *Lo_l=Loam low end variations; Lo_m=Loam mean variation; L_ma=Loam up end variatons; SaLo_l=Sandy Loam low end variations; SaLo_m=Sandy Loam mean variation; SaLo_ma=Sandy Loam up end variations; SaClLo_l=Sandy Clay Loam low end variations; SaClLo_m=Sandy Clay Loam mean variation; SaClLo_ma=Sandy Clay Loam up end variations.*

Overall, the results of the WF analysis showed that the optimal irrigation scenario achieved to considerably reduce the total WF of the maize crop and increased the rational use of the study area available water resources in the study area. This improvement is mostly attributed to the fact that in the case of optimized irrigation, the contribution of the green WF component was larger than that in the case of empirical irrigation. Moreover, a most consistent WF performance was observed when the former irrigation scenario was implemented, even among the years, showing that this approach can be used as a mean by the governmental public services to define maize crop benchmark WF limits for e.g., new CAP 2023-27 conditionality targes and thus use a meaningful way to evaluate the farmer performance realistically.

4 References

Beddington, J., 2009. Food, Energy, Water and the Climate: a Perfect Storm of Global Events? Speech given at Sustainable Development UK 2009. Available at. QEII Conference Center, London. Accessed 22/01/2020. https://webarchive.nationalarchives.gov.uk/20121206120858/ http://www.bis.gov.uk/assets/goscience/docs/p/perfect-storm-paper.pdf

Abd-Elmabod, S.K., Muñoz-Rojas, M., Jordán, A., Anaya-Romero, M., Phillips, J.D., Laurence, J., Zhang, Z., Pereira, P., Fleskens, L., van der Ploeg, M., de la Rosa, D., 2020. Climate change impacts on agricultural suitability and yield reduction in a Mediterranean region. Geoderma 374. https://doi.org/10.1016/j.geoderma.2020.114453

Ashapure, A., Jung, J., Chang, A., Oh, S., Maeda, M., Landivar, J., 2019. A comparative study of RGB and multispectral sensor-based cotton canopy cover modelling using multi-temporal UAS data. Remote Sens (Basel) 11. https://doi.org/10.3390/rs11232757

Bellón, B., Bégué, A., Seen, D. Lo, de Almeida, C.A., Simões, M., 2017. A remote sensing approach for regional-scale mapping of agricultural land-use systems based on NDVI time series. Remote Sens (Basel) 9, 1–17. https://doi.org/10.3390/rs9060600

Cao, X., Wu, P., Wang, Y., Zhao, X., 2014. Water Footprint of Grain Product in Irrigated Farmland of China. Water Resources Management 28, 2213–2227. https://doi.org/10.1007/s11269-014-0607-1

Chukalla, A.D., Krol, M.S., Hoekstra, A.Y., 2015. Green and blue water footprint reduction in irrigated agriculture: Effect of irrigation techniques, irrigation strategies and mulching. Hydrol Earth Syst Sci 19, 4877–4891. https://doi.org/10.5194/hess-19-4877-2015

D'Ambrosio, E., Gentile, F., de Girolamo, A.M., 2020. Assessing the sustainability in water use at the basin scale through water footprint indicators. J Clean Prod 244. https://doi.org/10.1016/j.jclepro.2019.118847

Frolking, S., Qiu, J., Boles, S., Xiao, X., Liu, J., Zhuang, Y., Li, C., Qin, X., 2002. Combining remote sensing and ground census data to develop new maps of the distribution of rice agriculture in China. Global Biogeochem Cycles 16, 38-1-38–10. https://doi.org/10.1029/2001gb001425

Han, C., Zhang, B., Chen, H., Liu, Y., Wei, Z., 2020. Novel approach of upscaling the FAO AquaCrop model into regional scale by using distributed crop parameters derived from remote sensing data. Agric Water Manag 240, 106288. https://doi.org/10.1016/j.agwat.2020.106288

Heyl, K., Döring, T., Garske, B., Stubenrauch, J., Ekardt, F., 2021. The Common Agricultural Policy beyond 2020: A critical review in light of global environmental goals. Rev Eur Comp Int Environ Law 30, 95–106. https://doi.org/10.1111/reel.12351

Hoekstra, A.Y., 2017. Water Footprint Assessment: Evolvement of a New Research Field. Water Resources Management 31, 3061–3081. https://doi.org/10.1007/s11269-017-1618-5

Hoekstra, A.Y., Mekonnen, M.M., 2012. The water footprint of humanity. Proceedings of the National Academy of Sciences 109, 3232 LP – 3237. https://doi.org/10.1073/pnas.1109936109

Karandish, F., Salari, S., Darzi-Naftchali, A., 2015. Application of Virtual Water Trade to Evaluate Cropping Pattern in Arid Regions. Water Resources Management 29, 4061–4074. https://doi.org/10.1007/s11269-015-1045-4

Kussul, N., Lavreniuk, M., Skakun, S., Shelestov, A., 2017. Deep Learning Classification of Land Cover and Crop Types Using Remote Sensing Data. IEEE Geoscience and Remote Sensing Letters 14, 778–782. https://doi.org/10.1109/LGRS.2017.2681128

Nouri, H., Stokvis, B., Galindo, A., Blatchford, M., Hoekstra, A.Y., 2019. Water scarcity alleviation through water footprint reduction in agriculture: The effect of soil mulching and drip irrigation. Science of the Total Environment 653, 241–252. https://doi.org/10.1016/j.scitotenv.2018.10.311

Prathumchai, K., Nagai, M., Tripathi, N.K., Sasaki, N., 2018. Forecasting transplanted rice yield at the farm scale using moderate-resolution satellite imagery and the aquacrop model: A case study of a rice seed production community in Thailand, in: ISPRS International Journal of Geo-Information. MDPI AG. https://doi.org/10.3390/ijgi7020073

Ranghetti, L., Boschetti, M., Nutini, F., Busetto, L., 2020. “sen2r”: An R toolbox for automatically downloading and preprocessing Sentinel-2 satellite data. Comput Geosci 139. https://doi.org/10.1016/j.cageo.2020.104473

Rocha, J., Carvalho-Santos, C., Diogo, P., Beça, P., Keizer, J.J., Nunes, J.P., 2020. Impacts of climate change on reservoir water availability, quality and irrigation needs in a water scarce Mediterranean region (southern Portugal). Science of the Total Environment 736. https://doi.org/10.1016/j.scitotenv.2020.139477

Saxton, K.E., Rawls, W.J., 2006. Soil Water Characteristic Estimates by Texture and Organic Matter for Hydrologic Solutions. Soil Science Society of America Journal 70, 1569–1578. https://doi.org/10.2136/sssaj2005.0117

Siad, S.M., Iacobellis, V., Zdruli, P., Gioia, A., Stavi, I., Hoogenboom, G., 2019. A review of coupled hydrologic and crop growth models. Agric Water Manag 224, 105746. https://doi.org/10.1016/j.agwat.2019.105746

Sui, R., Thomasson, J.A., Hanks, J., Wooten, J., 2008. Ground-based sensing system for weed mapping in cotton. Comput Electron Agric 60, 31–38. https://doi.org/10.1016/j.compag.2007.06.002

Tenreiro, T.R., García-Vila, M., Gómez, J.A., Jimenez-Berni, J.A., Fereres, E., 2020. Water modelling approaches and opportunities to simulate spatial water variations at crop field level. Agric Water Manag 240, 106254. https://doi.org/10.1016/j.agwat.2020.106254

Todaro, V., D’Oria, M., Secci, D., Zanini, A., Tanda, M.G., 2022. Climate Change over the Mediterranean Region: Local Temperature and Precipitation Variations at Five Pilot Sites. Water (Switzerland) 14. https://doi.org/10.3390/w14162499

Tsakmakis, I.D., Gikas, G.D., Sylaios, G.K., 2021. Integration of Sentinel-derived NDVI to reduce uncertainties in the operational field monitoring of maize. Agric Water Manag 255, 106998. https://doi.org/10.1016/j.agwat.2021.106998

Tsakmakis, I. D., Gikas, G.D., Sylaios, G.K., 2021a. Integration of Sentinel-derived NDVI to reduce uncertainties in the operational field monitoring of maize. Agric Water Manag 255, 106998. https://doi.org/10.1016/j.agwat.2021.106998

Tsakmakis, I. D., Gikas, G.D., Sylaios, G.K., 2021b. Integration of Sentinel-derived NDVI to reduce uncertainties in the operational field monitoring of maize. Agric Water Manag 255. https://doi.org/10.1016/j.agwat.2021.106998

Tsakmakis, I.D., Kokkos, N.P., Gikas, G.D., Pisinaras, V., Hatzigiannakis, E., Arampatzis, G., Sylaios, G.K., 2019. Evaluation of AquaCrop model simulations of cotton growth under deficit irrigation with an emphasis on root growth and water extraction patterns. Agric Water Manag 213, 419–432. https://doi.org/10.1016/j.agwat.2018.10.029

Tsakmakis, I.D., Zoidou, M., Gikas, G.D., Sylaios, G.K., 2018. Impact of Irrigation Technologies and Strategies on Cotton Water Footprint Using AquaCrop and CROPWAT Models. Environmental Processes 5, 181–199. https://doi.org/10.1007/s40710-018-0289-4

Tuel, A., Eltahir, E.A.B., 2020. Why Is the Mediterranean a Climate Change Hot Spot? J Clim 33, 5829–5843. https://doi.org/10.1175/JCLI-D-19

Veerakachen, W., Raksapatcharawong, M., 2020. RiceSAP: An Efficient Satellite-Based AquaCrop Platform for Rice Crop Monitoring and Yield Prediction on a Farm- To Regional-Scale. Agronomy 10. https://doi.org/10.3390/agronomy10060858

Wardlow, B.D., Egbert, S.L., 2008. Large-area crop mapping using time-series MODIS 250 m NDVI data: An assessment for the U.S. Central Great Plains. Remote Sens Environ 112, 1096–1116. https://doi.org/10.1016/j.rse.2007.07.019

Xu, R., Li, C., Paterson, A.H., 2019. Multispectral imaging and unmanned aerial systems for cotton plant phenotyping. PLoS One 14. https://doi.org/10.1371/journal.pone.0205083

Zaitunah, A., Samsuri, S., Ahmad, A.G., Safitri, R.A., 2018. Normalized difference vegetation index (ndvi) analysis for land cover types using landsat 8 oli in besitang watershed, Indonesia, in: IOP Conference Series: Earth and Environmental Science. Institute of Physics Publishing. https://doi.org/10.1088/1755-1315/126/1/012112

Zeng, Z., Liu, J., Koeneman, P.H., Zarate, E., Hoekstra, A.Y., 2012. Assessing water footprint at river basin level: A case study for the Heihe River Basin in northwest China. Hydrol Earth Syst Sci 16, 2771–2781. https://doi.org/10.5194/hess-16-2771-2012

Zhuo, L., Mekonnen, M.M., Hoekstra, A.Y., Wada, Y., 2016. Inter- and intra-annual variation of water footprint of crops and blue water scarcity in the Yellow River basin (1961-2009). Adv Water Resour 87, 29–41. https://doi.org/10.1016/j.advwatres.2015.11.002